Competitive adsorption of xenon and argon in zeolite Na*A*. ^{129}Xe nuclear magnetic resonance studies and grand canonical Monte Carlo simulations

Cynthia J. Jameson
Department of Chemistry M/C-111, University of Illinois at Chicago, 845 W. Taylor, Chicago, Illinois 60607

A. Keith Jameson
Department of Chemistry, Loyola University, 6525 Sheridan Road, Chicago, Illinois 60626

Hyung-Mi Lim
Department of Chemistry M/C-111, University of Illinois at Chicago, 845 W. Taylor, Chicago, Illinois 60607

(Received 29 November 1994; accepted 18 October 1994)

Investigation of competitive adsorption is carried out using the Xe–Ar mixture in zeolite Na*A* as a model system. The Xe_n clusters are trapped in the alpha cages of this zeolite for times sufficiently long that it is possible to observe individual peaks in the NMR spectrum for each cluster while the Ar atoms are in fast exchange between the cages and also with the gas outside. The ^{129}Xe nuclear magnetic resonance spectra of 12 samples of varying Xe and Ar loadings have been observed and analyzed to obtain the ^{129}Xe chemical shifts and the intensities of the peaks which are dependent on the average argon and xenon occupancies. The detailed distributions, $f(Xe_nAr_m)$, the fractions of cages containing n Xe atoms and m Ar atoms cannot be observed directly in this system, that is, individual peaks for Xe_nAr_m mixed clusters are not observed in the NMR spectrum. This information is, however, convoluted into the observed ^{129}Xe chemical shifts for the Xe_n peaks and the distributions P_n, the fraction of cages containing n Xe atoms, regardless of the number of Ar atoms, obtained from their relative intensities. Grand canonical Monte Carlo (GCMC) simulations of mixtures of Xe and Ar in a rigid zeolite Na*A* lattice provide the detailed distributions and the average cluster shifts, as well as the distributions P_n. The agreement with experiment is reasonably good for all 12 samples. The calculated absolute chemical shifts for the Xe_n peaks in all samples at 300 K range from 75 to 270 ppm and are in good agreement with experiment. The GCMC results are compared with a strictly statistical model of a binary mixture, derived from the hypergeometric distribution, in which the component atoms are distinguishable but equivalent in competition for eight lattice sites per cage under mutual exclusion. The latter simple model introduced here provides a limiting case for the distributions, with which both the GCMC simulations and the properties of the actual Xe–Ar system are compared. © *1996 American Institute of Physics.* [S0021-9606(96)50904-X]

INTRODUCTION

Microporous solids, zeolites in particular, are widely used in heterogeneous catalytic processes, separations, oil recovery, and other industrial processes.[1–3] A microscopic understanding of elementary processes at surfaces, such as adsorption and diffusion is an important fundamental problem and may assist in interpreting more complicated surface chemistry. A simple rare-gas physisorption system is a good starting point to investigate the distribution and dynamic behavior of adsorbed species. For our model system we have chosen zeolite Na*A*. This is an aluminosilicate of formula $Na_{12}[(SiO_2)_{12}(AlO_2)_{12}]$ whose crystal structure is well characterized. The framework structure provides a simple cubic arrangement of contiguous large cages (alpha cages). A Na^+ ion in each of the six windows to the cages keep the Xe atoms adsorbed inside for sufficiently long residence times such that each Xe_n is observed as a distinct signal in the high resolution NMR spectrum.

What is the equilibrium distribution of sorbate molecules in a given microporous solid? What factors influence this distribution? Until recently,[4,5] there had been no experimental measurements to provide the distribution of molecules in zeolite cavities. In our laboratory, we have directly observed in zeolite Na*A* the fraction of alpha cages containing, one, two,..., up to eight xenon atoms per cage. This distribution is found to be dependent on xenon loading and temperature. Grand canonical Monte Carlo (GCMC) simulations of this system have reproduced not only the observed distributions but also the ^{129}Xe chemical shift of the individual Xe_n clusters and their temperature dependence.[6] We have also measured the individual rates of transport of Xe atoms from a cage containing eight Xe atoms into a cage containing six, for example, and discovered that it is different from the rate of transport of a Xe atom from a cage containing three Xe atoms into a cage containing four atoms,[7] as was also found independently by Pines *et al.*[8]

Adsorption and diffusion of single gases in zeolites have been well studied in comparison to the adsorption of gas mixtures. Since industrial adsorption processes involve adsorption from streams which have multiple components, and

since applications of zeolites in separations depend on competitive adsorption, fundamental studies of binary and more complex mixtures in zeolites is extremely relevant. In early work, competitive adsorption of O_2, CO, CH_4, N_2 in binary mixtures in zeolite 5*A*,[9,10] N_2 and CO_2 in silicalite,[11] and ternary mixtures of N_2, O_2 and Ar in zeolite 5*A*[12] have been reported. More recently, selectivity coefficients in the adsorption of binary mixtures of hydrocarbons and of CO_2–N_2 in silicalite,[13] binary mixtures of N_2, O_2, and Ar in zeolite NaCa*X*,[14] binary mixtures of cyclohexane with di-Me-pentane isomers in silicalite,[15] and binary and ternary mixtures of di-Me-naphthalene isomers in zeolite *X* and *Y*[16] have been found to be strongly dependent on the composition of the fluid phase. In selected instances,[16–18] the results of competitive adsorption has been discussed in terms of ideal adsorbed solution theory.[19] This theory, which considers the adsorbed phase to be an ideal solution where Raoult's law describes the binary sorption equilibria, is particularly useful for systems in which the molecular volumes of the components are similar.[10,11,20] The most detailed interpretation of binary mixtures in zeolites comes from grand Canonical Monte Carlo simulations, such as those which have been reported for N_2–O_2 mixtures in zeolite 5*A*,[21] for mixtures of CH_4–CO_2 and C_2H_4–CO_2 in zeolite *X*,[20] for CH_4–N_2 in Na*Y*[18,22] and for Xe–Ar, CH_4 in *A*-type zeolites.[23] However, besides the selectivity coefficients, there is little else resulting from these simulations that could be compared with experiment.

Changes in the ^{129}Xe chemical shifts due to the presence of other guest molecules in the cavities has raised the possibility of using Xe NMR as a means of characterizing the intrazeolitic distribution of the guest molecules.[24–26] However, these studies involve having the Xe in fast exchange and the guest molecules having very long residence times in the cavities, thus, only a single Xe peak can be observed and its chemical shift is an average over *all* cavity occupancies for the guest and for the xenon atoms. Before any quantitative applications can be made of this method, more detailed information about the distribution of Xe and the coadsorbate among the cavities is crucial, yet there have been no studies that shed light on this question.

What is the role played by coadsorbates in the distribution of one type of molecule throughout the microporous solid? In the ideal case, we expect to be able to measure directly the equilibrium distribution of molecules of one type in cages containing only one, or exactly two, or some other known number of molecules of a second type. That is to say, it would be desirable to measure directly the fraction of zeolite cages containing *nA* molecules and *mB* molecules. Such detailed information together with the partial pressures or densities of the *A* and *B* in the gas in equilibrium with the adsorbed phase would provide a more complete description of competitive adsorption than has ever been available. We have indeed succeeded in the observation of mixed clusters Xe_nKr_m peaks in the ^{129}Xe NMR spectrum of Xe–Kr mixtures in zeolite Na*A*, from which peak intensities the detailed distributions can be directly obtained.[27] However, the range of Kr occupancies in which this can be done is rather narrow due to unfavorable cage-to-cage migration rates of Kr for mixed clusters having more than one Kr atom. In this paper, we investigate the Xe–Ar competitive adsorption in zeolite Na*A*, in which the Ar atoms are in fast exchange while the Xe_n clusters remain in the cages during the NMR measurements. These studies cover a broad range of average occupancies and provide detailed information at the intermediate level since each Xe_n cluster is observed in the presence of average numbers of Ar atoms, a different average number for each Xe_n cluster size, which we shall denote as $[\langle m\rangle_{\mathrm{Ar}}]_n$. We obtain the ^{129}Xe NMR chemical shifts for each Xe_n cluster as well as direct measures of P_n, the fraction of zeolite alpha cages that contain *n* Xe atoms regardless of the number of Ar atoms. We report grand canonical Monte Carlo simulations of this system and also consider a strictly statistical model of a binary mixture, derived from the hypergeometric distribution, in which the component atoms are distinguishable but equivalent in competition for eight lattice sites per cage, subject to mutual exclusion.

EXPERIMENTAL AND COMPUTATIONAL METHODS

Definitions

Let the fraction $f(n,m)\equiv f(\mathrm{Xe}_n\mathrm{Ar}_m)$ be the fraction of the alpha cages containing *n* Xe atoms and *m* Ar atoms. The observed intensities of the Xe_n cluster peaks is related to the fractions of alpha cages containing *n* Xe atoms regardless of the number of Ar atoms, which is given by,

$$P_n=\sum_{m=0} f(n,m).$$

Note that the fraction of ''empty'' cages (having zero Xe atoms and therefore no observable intensity in the ^{129}Xe NMR spectra) includes the truly empty cages as well as all those occupied by various numbers of Ar atoms,

$$P_0=\sum_{m=0} f(0,m).$$

Similarly, if the ^{129}Xe shieldings of mixed clusters Xe_nAr_m are known independently, then the average shielding of Xe_n in a mixture having average occupancies $\langle n\rangle$ of Xe and $\langle m\rangle$ of Ar is given by,

$$\langle\sigma(\mathrm{Xe}_n\mathrm{Ar}_{\mathrm{ave}})\rangle=\sum_{m=0}\sigma(\mathrm{Xe}_n\mathrm{Ar}_m)f(\mathrm{Xe}_n\mathrm{Ar}_m)\Big/\sum_{m=0} f(\mathrm{Xe}_n\mathrm{Ar}_m).$$

The quantity on the left is the observed ^{129}Xe shielding for the Xe_n cluster including some average number of Ar atoms under fast exchange, which depends on the overall $\langle n\rangle$ of Xe and $\langle m\rangle$ of Ar in each sample. On the other hand, the ^{129}Xe shieldings in the individual mixed clusters Xe_nAr_m do not depend on the Xe or Ar loading, as we may assume from the observed invariance of the ^{129}Xe shieldings for the individual Xe_n clusters to Xe loading in the pure xenon adsorbed in Na*A*.[5] It will be found in this work that the average ^{129}Xe

shielding in the mixed clusters having the same number of Xe atoms changes monotonically with each additional Ar, producing what could be considered a progression. Thus this equation provides a way by which the changes in the observed Xe chemical shifts with loading may be understood.

Because of the progression of the ^{129}Xe shieldings with increasing m in the mixed clusters Xe_nAr_m, it is helpful to consider the average $\langle m\rangle_{Ar}$ corresponding to only those cages having specifically n Xe atoms, which we designate as $[\langle m\rangle_{Ar}]_n$. This is, of course, given by

$$[\langle m\rangle_{Ar}]_n = \sum_{m=0} mf(Xe_nAr_m) \Big/ \sum_{m=0} f(Xe_nAr_m).$$

At a given temperature, the observed average shielding for those cages having n Xe atoms will differ from that observed for Xe_n in the pure xenon samples by an amount that is determined entirely by $[\langle m\rangle_{Ar}]_n$.

Sample preparation and high resolution NMR

Sample preparation has been previously described.[5] Four mm (o.d.) tubes are fashioned from ordinary borosilicate tubing, containing a volume of 0.20–0.25 mL, calibrated with mercury. A known mass of zeolite is introduced (typically 50 mg), dried for 16 h under ''thin-bed'' conditions at 350–400 °C under vacuum. A known number of moles of Xe and Ar are introduced and the sample is flame-sealed under liquid nitrogen. The mass balance of Xe and Ar between the adsorbed and gaseous phases can be obtained from NMR data in an experimental manner. Measuring the intensity of the Xe signal in the gas phase of the inverted tube (positioned carefully and reproducibly in the receiver coil) yields the density of gaseous xenon in the tube. Care must be taken that the longitudinal relaxation time of the sample is adequately considered. This allows the mass-balance determination of xenon between the gaseous and adsorbed phases.

Spectra were taken on a Bruker AM-400 spectrometer, temperature-controlled at 300 K using the ^{1}H spectrum of neat ethylene glycol as a secondary temperature standard. The spectrometer was run unlocked (magnet drift is negligible) with the field adjusted so that the resonance frequency of the methylene group of ethylene glycol is at 400.139 015 MHz. A pulse width of 22.5 μs (90° pulse) was used with a 10 s relaxation delay. Our earlier magnetization transfer experiments[7] showed us that the experimental relaxation time of all Xe_n clusters in a given sample is identical due to cage-to-cage migration. Thus the relative peak intensities of Xe_n in these specific systems are reliable over a wide range of recycle times. Typically 500–8000 scans were collected for the spectra of ^{129}Xe in the zeolite. Much greater care was needed with regard to obtaining reliable intensities for the gas peak where densities may be low and Xe relaxation times relatively long. 30° pulse widths and recycle delays of 60 s insure that intensities are reliable within a relative error of 10% even if T_1=60 s. In our samples there are heterogeneous mechanisms or other minor sources for relaxation for ^{129}Xe in the gas phase, which help to shorten T_1. Typical ^{129}Xe high resolution NMR spectra are shown in Fig. 1.

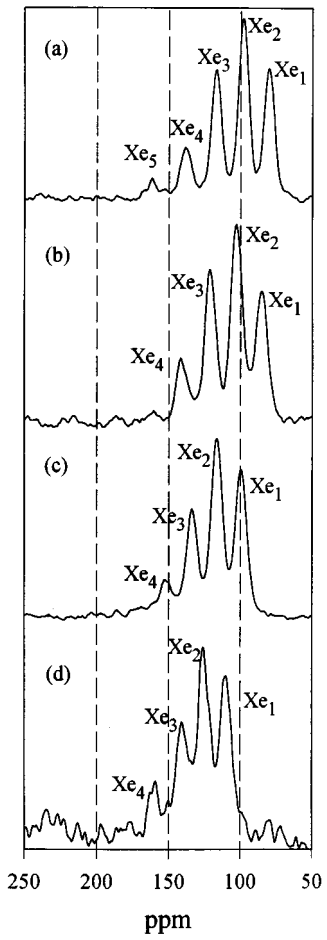

FIG. 1. Typical ^{129}Xe NMR spectra of mixtures of Xe and Ar at equilibrium in dehydrated zeolite Na*A*. The Xe and Ar loadings in these samples are (a) $\langle n\rangle_{Xe}$=1.54, $\langle m\rangle_{Ar}$=0.86; (b) $\langle n\rangle_{Xe}$=1.36, $\langle m\rangle_{Ar}$=1.65; (c) $\langle n\rangle_{Xe}$=1.22, $\langle m\rangle_{Ar}$=3.60; (d) $\langle n\rangle_{Xe}$=1.23, $\langle m\rangle_{Ar}$=4.79.

Determination of overall $\langle n\rangle_{Xe}$ and overall $\langle m\rangle_{Ar}$

The fractions P_n of cages containing n Xe atoms regardless of the number of Ar atoms are observable quantities, derived from the integrated intensities of the Xe_n peaks just as in the pure xenon case.[5] The experimental distribution of occupancies of the alpha cages were obtained by fitting the spectra to a combination of Lorentzian/Gaussian functions (GRAMS, Galactic Industries, Salem, NH). The spectroscopic $\langle n\rangle_{Xe}$ is directly obtained from the areas A_n of the Xe_n peaks. If we let $g(n)$ be the fraction of *those cages occupied by Xe atoms* which contain n Xe atoms,

$$g(n) = (A_n/n)\sum_{k=1} (A_k/k),$$

$$\langle n\rangle_{Xe,\ spectrosc} = \sum_{k=1} kg(k).$$

The fraction of *all alpha cages* containing n Xe atoms, P_n, is the same as $g(n)$ when all cages contain at least one Xe atom. P_n differs from $g(n)$ only very slightly for xenon loadings $\langle n\rangle_{Xe}>4.0$. When the $\langle n\rangle_{Xe}<4.0$ the relative inten-

sities together with the spectroscopic $\langle n\rangle_{\mathrm{Xe}}$ obtained from them provide the fractions of cages which are occupied by Xe atoms if the xenon loading $\langle n\rangle_{\mathrm{Xe}}$ is known, from xenon mass balance, for example. The relation between these two sets of quantities is, of course,

$$(1-P_0)=\langle n\rangle_{\mathrm{Xe}}/\langle n\rangle_{\mathrm{Xe,\ spectrosc}},$$

$$P_n=(1-P_0)g(n).$$

Although mass balance provides P_0, it becomes much more difficult to determine the Xe density in the gas phase accurately because the bulk gas in equilibrium with the adsorbed atoms is a mixture. For those samples in which the overall $\langle n\rangle_{\mathrm{Xe}}$ can also be obtained spectroscopically, i.e., when all cages contain at least one Xe atom, the values of $\langle n\rangle_{\mathrm{Xe}}$ obtained directly from the intensities of the Xe_n peaks and those obtained from mass balance should be identical, and we use the spectroscopic $\langle n\rangle_{\mathrm{Xe}}$ in these cases. For the other samples, we use the hypergeometric distribution to find the fraction P_0 of empty cages from the spectroscopic $\langle n\rangle_{\mathrm{Xe}}$. This procedure then allows us to determine a more accurate experimental $\langle n\rangle_{\mathrm{Xe}}$ for the sample than we can obtain from Xe mass balance and we shall see later (in the penultimate figure) that this procedure is entirely justified.

Now, about the determination of the overall $\langle m\rangle_{\mathrm{Ar}}$ in the Xe–Ar coadsorption in Na*A*. In principle, given the density of the Xe in the gas phase outside the zeolite crystallites, and the ^{129}Xe chemical shift of the gas peak, it should be possible to determine indirectly the density of Ar in the gas phase, since the ^{129}Xe chemical shift behavior in all-gas mixtures of Xe and Ar has previously been established. The relation is given by,

$$\sigma(T,\rho)=\sigma_0(T)+\sigma_1(T)_{\mathrm{Xe-Xe}}\rho_{\mathrm{Xe}}+\sigma_1(T)_{\mathrm{Xe-Ar}}\rho_{\mathrm{Ar}}+\cdots,$$

where $\sigma(T,\rho)$ is the shielding in the gas mixture, $\sigma_0(T)$ is the shielding of an isolated Xe atom, $\sigma_1(T)_{\mathrm{Xe-Xe}}$ is the second virial coefficient of the Xe shielding due to Xe–Xe interactions, and $\sigma_1(T)_{\mathrm{Xe-Ar}}$ is the second virial coefficient of the Xe shielding due to Xe–Ar interactions, which have previously been published.[28] Using ρ_{Xe} from the intensity of the gas peak, we could subtract out the Xe–Xe contributions to the gas peak shift, to leave the Xe–Ar contributions and thereby calculate ρ_{Ar}. By mass balance of Ar atoms, the overall $\langle m\rangle_{\mathrm{Ar}}$ can then be obtained. This procedure, however, would leave all the errors coming from the various measurements (total moles of Ar in the sample, total moles of Xe in the sample, gas peak intensity, gas peak chemical shift, $\sigma_1(T)_{\mathrm{Xe-Xe}}$, and $\sigma_1(T)_{\mathrm{Xe-Ar}}$) in the value of the overall $\langle m\rangle_{\mathrm{Ar}}$. This is a particularly severe problem for low $\langle m\rangle_{\mathrm{Ar}}$ since the Xe shift due to Xe–Ar interactions is only about a third of that due to Xe–Xe interactions.[28] Therefore, we considered the following alternative. If we know the average ^{129}Xe chemical shifts of the mixed clusters $\mathrm{Xe}_n\mathrm{Ar}_m$ (these shieldings are averaged only within the cage and are not affected by the distribution of the Xe and Ar atoms among the alpha cages) then we can estimate the effective average number of Ar atoms in the cages containing specifically *n* Xe atoms, that is, $[\langle m\rangle_{\mathrm{Ar}}]_n$, from the experimental chemical shift of the individual Xe_n peaks. This is done for each Xe_n chemical shift independently. The $[\langle m\rangle_{\mathrm{Ar}}]_0$ (for the cages containing no Xe atoms) is obtained by linear extrapolation from the values for the cages containing Xe_2 and Xe_1. These individual $[\langle m\rangle_{\mathrm{Ar}}]_n$ are then weighted by P_n in computing the overall $\langle m\rangle_{\mathrm{Ar}}$ for the sample, which is used as the experimental value. For this purpose, the shieldings of the mixed cluster $\mathrm{Xe}_n\mathrm{Ar}_m$ are obtained from averaging of the *ab initio*-derived Xe–Xe and the Xe–Ar shielding functions[29] within the cage.

Grand canonical Monte Carlo simulations

The grand canonical ensemble is appropriate for adsorption systems, in which the adsorbed phase is in equilibrium with the gas at some specified temperature. The use of a computer simulation allows us to calculate average macroscopic properties directly without having to explicitly calculate the partition function. The grand canonical Monte Carlo (GCMC) method as applied in this work has been described in detail earlier,[6] so only the aspects involving binary fluid mixtures will be mentioned here. Cut-and-shifted Lennard-Jones (12–6) potentials were used to model the interactions between rare gas–oxygen and rare gas–Na. These effective potentials describe the interaction between the adsorbed fluid and the zeolite; the Si and Al atoms are not directly involved in the simulation, their influence being incorporated into the parameters of the rare gas–oxygen potential, which are dependent on the Si/Al ratio. The Xe–O and Xe–Na parameters are unchanged from our previous work on Xe in Na*A*.[6] The Ar–O and Ar–Na parameters were obtained by adjusting to the adsorption isotherms of pure argon in Na*A* at 195 K and 303 K,[30,31] starting from the initial parameter set used by Kiselev and Du for Na*X*.[32] The set $r_0=3.0$ Å, $\epsilon/k=159.24$ K for Ar–O and $r_0=3.236$ Å, $\epsilon/k=35.82$ K for Ar–Na gives simulated adsorption isotherms that are in good agreement with experimental data at both temperatures. The Xe–Xe potential used is of the Maitland–Smith form, as described in our previous simulations of Xe in Na*A*, fitted to the best available Xe–Xe potential of Aziz and Slaman.[6,33] Likewise the Xe–Ar and the Ar–Ar potentials were taken from the best available potentials of Aziz *et al.*,[34,35] and fitted to the Maitland–Smith form. The values of m and γ were initially taken from the recommended set of Maitland *et al.*[36] Final values used in this work are $m=13$, $\gamma=8.0$ for Xe–Ar and $m=13$, $\gamma=7.5$ for Ar–Ar. A minimum separation was imposed on all pairs of interacting atoms, corresponding to the distance at which the potential energy is equal to $5kT$, the probability of configurations involving shorter distances being less than $\exp(-5)$. This is employed to save computational time by excluding configurations that are extremely unlikely. The simulation box is a unit cell of zeolite Na*A*, with the atomic coordinates, including the Na cations, taken from the x-ray single crystal refinement of the dehydrated zeolite by Pluth and Smith.[37] This is unchanged from our previous work.[6] Periodic boundary conditions were imposed using the minimum image convention, consistent with the

cut-and-shifted potentials employed.[38] The Markov chain is constructed using the Norman–Filinov method, that is, using three equally weighted types of moves, one involving displacement of a particle, and two moves randomly chosen from destruction or creation of a particle,[39] a technique used by Woods and Rowlinson[40] and in our previous work.[6] The core of the program effects the creation/destruction and displacement of one atom at a time and calculates the associated energy change, ΔU in each case. This is used to continuously update the total configurational energy of the system, without having to recalculate every interaction at every step. The displacement step uses the adsorbed phase composition in the choice of either fluid. The creation/destruction step begins with the decision to either create or destroy a particle. If the decision is to destroy a particle (that is, the particle is assumed to go into the gas phase) the choice between destroying an atom of Xe or Ar is made proportionately to the gas phase composition, i.e., ρ_{Xe} and ρ_{Ar}. If the decision is to create a particle (i.e., remove it from the bulk gas and place it in the zeolite), the choice of creating an atom of Xe or Ar is made according to the gas phase composition. A single atom of the chosen fluid is then created at a random position in the zeolite. Therefore, it is necessary to know *a priori* the ratio of the gas densities in equilibrium with the adsorbed phase before the simulation starts. This is easily done by first calculating the chemical potential of the Xe and the Ar appropriate to the temperature and densities in the gas mixture, using the virial coefficients,

$$\mu_1-\mu_1^0=2RT(\rho_1B_{11}+\rho_2B_{12})+RT\ \ln(\rho_1/\rho^0),$$

$$\mu_2-\mu_2^0=2RT(\rho_2B_{22}+\rho_1B_{12})+RT\ \ln(\rho_2/\rho^0).$$

These values of the chemical potential are the same for the adsorbed phase with which the gas mixture is in equilibrium. These chemical potentials, the temperature, and the mole fraction of Xe in the gas are the parameters of a GCMC simulation. Consistent with the above equations, the pressure of the gas is calculated using the virial equation of state,

$$P=RT(\rho+\rho_1^2B_{11}+2\rho_1\rho_2B_{12}+\rho_2^2B_{22})$$

and the configurational energy of the bulk gas mixture is calculated by

$$U_{\mathrm{gas}}=-RT^2\rho[y_1^2(dB_{11}/dT)+2y_1y_2(dB_{12}/dT)+y_2^2(dB_{22}/dT)],$$

where y_1 and y_2 are the mole fractions in the binary gas mixture. The virial coefficients used in this work were taken from Dymond and Smith[41] and Brewer[42] and are reproduced by the Maitland–Smith potential functions used here.

The ^{129}Xe shielding, like the energy, is taken to be expressible as a sum of pairwise contributions, using atom–atom shielding functions that are likewise cut and shifted. The Xe–O and Xe–Na shielding functions are based on *ab initio* calculations on model systems and are the same as was used in our previous work.[6] The Xe–Xe and the Xe–Ar shielding functions are based on *ab initio* calculations and are taken from Ref. 29. These have been shown to reproduce reasonably well the temperature dependent density coefficients of the ^{129}Xe chemical shifts for pure xenon gas and for Xe in Ar gas mixtures. At each step in the simulation at which the atom–atom interaction energy is calculated, the shielding contribution is calculated too, when one of the atoms involved is a xenon atom. Since the shielding functions go to large negative values at close approach, it is quite important to have Xe–Xe and Xe–Ar potentials that have the correct behavior at these short distances, especially close to r_0. This is the reason for using accurate two-body potentials rather than Lennard-Jones for Xe–Xe and Xe–Ar. The Maitland–Smith form provides a superior fit to the best Aziz potentials and is just as inexpensive as the Lennard-Jones form in computational overhead.

The results of the GCMC simulations are analyzed to provide the usual one-body distribution functions, pair distribution functions, and occupancies. In addition, the average shieldings for individual mixed clusters Xe_nAr_m, which are independent of loading, are accumulated over all the GCMC runs, as well as the averages for Xe_n clusters for each (μ_1,μ_2,T). All calculations reported here were carried out on IBM RISC/6000 (models 560 and 365) workstations.

RESULTS

The experimental and simulation results reported here are for twelve samples equilibrated at 300 K. Just as for pure Xe in Na*A*, the exchange rate for Xe atoms from one cage to another is slow enough that distinct assignable peaks corresponding to 1,2,3,...8 Xe atoms in a cage are observed. The peaks corresponding to the n Xe atoms in an alpha cage in the Xe and Ar mixture in Na*A* have the same line widths as the Xe_n peaks observed in pure Xe in Na*A*; the Ar appears to be in fast exchange at 300 K in these samples. Typical spectra are shown in Fig. 1. Note how the Xe_n chemical shifts change with Ar loading. In Tables I and II and Fig. 2 and 3 we present the experimental results for the twelve samples with various loadings of Xe and Ar in zeolite Na*A*.

Experimental ^{129}Xe chemical shifts and distributions of xenon atoms

The distributions, the fractions P_n of the alpha cages containing n Xe atoms, which have been obtained from the peak intensities, are given in Table I and in Fig. 2. The general trend observed in the distributions is that P_n is largely determined by $\langle n\rangle_{\mathrm{Xe}}$, and only secondarily by $\langle m\rangle_{\mathrm{Ar}}$, if at all.

The ^{129}Xe chemical shifts for Xe_n clusters are given in Table II and in Fig. 3. We report the difference in chemical shift between the Xe_n peak in the Xe–Ar mixture in Na*A* and the Xe_n peak in pure xenon in Na*A* as $\{\langle\sigma(Xe_nAr_{\mathrm{ave}})\rangle-\langle\sigma(Xe_n)\rangle\}$, to more effectively illustrate the effects of the coadsorption. For a given sample, the larger the number of xenon atoms in the cluster the smaller the chemical shift relative to the Xe_n in pure xenon in Na*A*. We note in Fig. 3 that in comparing samples with different Ar loadings, the larger the cluster, the smaller the change in $\{\langle\sigma(Xe_nAr_{\mathrm{ave}})\rangle-\langle\sigma(Xe_n)\rangle\}$ with increasing overall $\langle m\rangle_{\mathrm{Ar}}$ of

TABLE I. The Xe distribution in mixtures of Xe–Ar in Na*A*: P_n, the fractions of alpha cages containing n Xe atoms.

Xe_0	Xe_1	Xe_2	Xe_3	Xe_4	Xe_5	Xe_6	Xe_7	Xe_8	$\langle n\rangle_{Xe}$	$\langle m\rangle_{Ar}$
Experimental										
0.425	0.391	0.139	0.038	0.007	0.00	0.00	0.00	0.00	0.81	1.24
0.266	0.396	0.221	0.088	0.030	0.00	0.00	0.00	0.00	1.22	3.60
0.263	0.395	0.222	0.090	0.031	0.00	0.00	0.00	0.00	1.23	4.79
0.246	0.370	0.259	0.103	0.022	0.00	0.00	0.00	0.00	1.28	2.14
0.226	0.380	0.232	0.132	0.030	0.00	0.00	0.00	0.00	1.36	1.65
0.181	0.363	0.267	0.127	0.046	0.015	0.00	0.00	0.00	1.54	0.86
0.080	0.231	0.308	0.239	0.116	0.027	0.00	0.00	0.00	2.16	2.99
0.069	0.208	0.295	0.257	0.136	0.036	0.00	0.00	0.00	2.29	1.15
0.058	0.204	0.284	0.257	0.139	0.046	0.012	0.00	0.00	2.40	3.09
0.034	0.154	0.233	0.285	0.196	0.080	0.018	0.00	0.00	2.77	1.85
0.00	0.00	0.00	0.00	0.111	0.308	0.403	0.178	0.00	5.65	0.68
0.00	0.00	0.00	0.00	0.00	0.135	0.410	0.375	0.080	6.40	0.17
GCMC results										
Xe_0	Xe_1	Xe_2	Xe_3	Xe_4	Xe_5	Xe_6	Xe_7	Xe_8	$\langle n\rangle_{Xe}$	$\langle m\rangle_{Ar}$
0.431	0.381	0.148	0.035	0.005	0.0004	0.0000	0.0000	0.0000	0.80	1.21
0.227	0.398	0.269	0.086	0.019	0.001	0.0000	0.0000	0.0000	1.28	3.53
0.255	0.408	0.238	0.074	0.024	0.001	0.0000	0.0000	0.0000	1.21	4.88
0.242	0.376	0.256	0.101	0.023	0.002	0.0000	0.0000	0.0000	1.29	2.11
0.239	0.355	0.260	0.113	0.030	0.001	0.0000	0.0000	0.0000	1.34	1.71
0.184	0.3336	0.285	0.148	0.045	0.005	0.0003	0.0000	0.0000	1.55	0.92
0.071	0.2389	0.323	0.243	0.099	0.022	0.003	0.0000	0.0000	2.14	3.05
0.060	0.1987	0.301	0.266	0.134	0.036	0.004	0.0000	0.0000	2.34	1.20
0.039	0.178	0.307	0.300	0.145	0.028	0.003	0.0000	0.0000	2.43	3.14
0.028	0.1309	0.266	0.303	0.191	0.069	0.011	0.0008	0.0000	2.75	1.88
0.0000	0.0000	0.0006	0.012	0.092	0.317	0.424	0.146	0.009	5.63	0.62
0.0000	0.0000	0.0001	0.0005	0.007	0.106	0.421	0.388	0.079	6.42	0.23
Hypergeometric model results										
Xe_0	Xe_1	Xe_2	Xe_3	Xe_4	Xe_5	Xe_6	Xe_7	Xe_8	$\langle n\rangle_{Xe}$	$\langle m\rangle_{Ar}$
0.4257	0.3837	0.1513	0.0341	0.0048	0.0004	0.0000	0.0000	0.0000	0.81	1.24
0.2661	0.3831	0.2413	0.0868	0.0195	0.0028	0.0002	0.0000	0.0000	1.22	3.60
0.2624	0.3821	0.2435	0.0886	0.0202	0.0029	0.0003	0.0000	0.0000	1.23	4.79
0.2464	0.3772	0.2526	0.0967	0.0231	0.0035	0.0003	0.0000	0.0000	1.28	2.14
0.2252	0.3690	0.2646	0.1084	0.0277	0.0045	0.0005	0.0000	0.0000	1.36	1.65
0.1808	0.3448	0.2877	0.1371	0.0409	0.0078	0.0010	0.0001	0.0000	1.54	0.86
0.0806	0.2386	0.3089	0.2285	0.1056	0.0313	0.0058	0.0006	0.0003	2.16	2.99
0.0674	0.2161	0.3033	0.2433	0.1220	0.0391	0.0078	0.0009	0.0000	2.29	1.15
0.0576	0.1976	0.2965	0.2541	0.1361	0.0467	0.0100	0.0012	0.0001	2.40	3.09
0.0335	0.1416	0.2623	0.2775	0.1835	0.0777	0.0205	0.0031	0.0002	2.77	1.85
0.0001	0.0011	0.0090	0.0432	0.1298	0.2495	0.2998	0.2058	0.0618	5.65	0.68
0.0000	0.0001	0.0011	0.0092	0.0459	0.1468	0.2936	0.3355	0.1678	6.40	0.17

the sample. For every Xe_n, the shielding in the presence of Ar relative to the Xe_n cluster in pure Xe, $\{\langle\sigma(Xe_nAr_{ave})\rangle-\langle\sigma(Xe_n)\rangle\}$ becomes more negative with increasing $\langle m\rangle_{Ar}$. This change becomes more exaggerated with increasing $\langle n\rangle_{Xe}$: in Fig. 3, note the difference between the low $\langle n\rangle_{Xe}$ points (○) and the high $\langle n\rangle_{Xe}$ points (●). That is, the ^{129}Xe chemical shifts relative to the pure xenon Xe_n cluster are largely determined by the overall $\langle m\rangle_{Ar}$ and only secondarily determined by $\langle n\rangle_{Xe}$ in mixtures of Xe and Ar in zeolite Na*A*. In contrast, the average cluster shifts $\langle\sigma(Xe_n)\rangle$ observed in pure xenon in Na*A* are completely independent of $\langle n\rangle_{Xe}$. This secondary dependence of the ^{129}Xe chemical shifts in mixtures of Xe and Ar in zeolite Na*A* on $\langle n\rangle_{Xe}$ is a very interesting feature of coadsorption which we will explore in detail.

Grand canonical Monte Carlo simulations

GCMC simulations were carried out for mixtures of various gas phase compositions (μ_1,μ_2,T), and the simulations most closely matching the experimental values of $\langle n\rangle_{Xe}$ and $\langle m\rangle_{Ar}$ are shown here for comparison with experiment. Each experimental sample has about 2×10^{19} alpha cages, whereas the GCMC simulations provide typically 2.4×10^{7} properly weighted snapshots of alpha cages. The fractions of alpha cages containing n Xe atoms obtained from the simulations are shown in Table I and Fig. 2. The simulations also provide the average number of Ar atoms associated with each individual Xe_n and these are shown in Table III. The results of the ^{129}Xe shielding calculations for the Xe_n clusters in the Xe–Ar mixture in Na*A* in the GCMC simulation are

TABLE II. ^{129}Xe chemical shifts, $\{\langle\sigma(Xe_nAr_{ave})\rangle-\langle\sigma(Xe_n)\rangle\}$, for Xe–Ar mixtures in Na*A*.

Experimental									
Xe_1	Xe_2	Xe_3	Xe_4	Xe_5	Xe_6	Xe_7	Xe_8	$\langle n\rangle_{Xe}$	$\langle m\rangle_{Ar}$
−5.4	−5.8	−5.4	−5.2	−3.6				1.54	0.86
−7.3	−7.6	−7.2	−5.6					0.81	1.24
−10.7	−10.6	−9.6	−7.9					1.36	1.65
−14.0	−13.7	−12.1	−10.2					1.28	2.14
−24.9	−24.3	−22.1	−19.0					1.22	3.60
−35.4	−33.5	−29.3	−27.1					1.23	4.79
−8.6	−9.0	−8.0	−6.7	−4.5				2.29	1.15
−17.2	−16.4	−14.7	−12.2	−8.2	−6.7			2.77	1.85
−24.8	−24.1	−21.4	−18.3	−13.1				2.16	2.99
−27.6	−26.5	−23.6	−20.2	−14.8	−11.4			2.40	3.09
			−16.8	−10.9	−7.9	−2.3		5.65	0.68
				−5.9	−3.3	−1.2	1.1	6.40	0.17
GCMC results									
Xe_1	Xe_2	Xe_3	Xe_4	Xe_5	Xe_6	Xe_7	Xe_8	$\langle n\rangle_{Xe}$	$\langle m\rangle_{Ar}$
−6.0	−6.8	−6.9	−5.5	−3.9				1.55	0.92
−7.5	−7.9	−9.5	−7.0					0.80	1.21
−10.3	−12.4	−12.5	−11.9	(−1.4)				1.34	1.71
−14.2	−13.9	−13.6	−11.0	(−6.6)				1.29	2.11
−26.1	−23.2	−22.9	−20.8	(−31.6)				1.28	3.53
−37.9	−35.8	−31.0	−23.4	(−31.6)				1.21	4.88
−8.6	−8.5	−9.0	−6.8	−7.2	(−6.6)			2.34	1.20
−17.0	−16.9	−15.7	−13.4	−9.0	−12.7	(−1.0)		2.75	1.88
−24.8	−24.9	−23.5	−23.4	−23.5	(−24.5)			2.14	3.05
−29.3	−27.8	−25.8	−21.1	−21.2	(−1.2)			2.43	3.14
		−14.4	−13.6	−11.1	−6.9	−2.9	−1.6	5.63	0.62
			−14.8	−7.1	−4.8	−1.0	−2.0	6.42	0.23
Hypergeometric model results									
Xe_1	Xe_2	Xe_3	Xe_4	Xe_5	Xe_6	Xe_7	Xe_8	$\langle n\rangle_{Xe}$	$\langle m\rangle_{Ar}$
−5.60	−5.60	−5.50	−5.40	−4.70	−4.50	−2.30	0.00	1.54	0.86
−7.40	−7.30	−7.30	−7.10	−6.20	−5.80	−3.00	0.00	0.81	1.24
−10.90	−10.80	−10.60	−10.30	−9.00	−8.40	−4.20	0.00	1.36	1.65
−14.20	−14.10	−13.90	−13.40	−11.70	−10.70	−5.40	0.00	1.28	2.14
−25.30	−24.80	−24.30	−23.10	−20.10	−17.80	−9.10	0.00	1.22	3.60
−35.60	−34.80	−33.60	−31.80	−27.40	−23.60	−12.10	0.00	1.23	4.79
−8.70	−8.60	−8.50	−8.30	−7.30	−6.80	−3.40	0.00	2.29	1.15
−15.90	−15.70	−15.50	−14.90	−13.10	−11.90	−6.00	0.00	2.77	1.85
−24.30	−23.80	−23.40	−22.30	−19.40	−17.20	−8.70	0.00	2.16	2.99
−26.50	−26.00	−25.40	−24.20	−21.00	−18.50	−9.40	0.00	2.40	3.09
−12.70	−12.60	−12.50	−12.00	−10.50	−9.70	−4.90	0.00	5.65	0.68
−4.50	−4.50	−4.50	−4.40	−3.80	−3.70	−1.90	0.00	6.40	0.17

compared with the GCMC simulations of pure Xe in the same simulation box and the resulting differences in shielding $\{\langle\sigma(Xe_nAr_{ave})\rangle-\langle\sigma(Xe_n)\rangle\}$ are shown in Table II. These differences may be compared directly with experiment, are a direct measure of the intermolecular effects of Ar, and are therefore a direct measure of the average number of Ar atoms in the cage with Xe_n. It should be noted that when the fraction of cages containing Xe_n in the sample is small, then the number of configurations over which the chemical shift is averaged may not be large enough to obtain a statistically valid average. The chemical shifts in those cages represented by $P_n<0.005$ are shown enclosed in parentheses in Table II and the chemical shifts in those cages represented by $P_n<0.0005$ are not shown at all.

In Fig. 4 the total intermolecular chemical shift measured relative to the isolated Xe atom, the ^{129}Xe chemical shift for Xe_n in an alpha cage with an average number of Ar atoms under fast exchange (which is directly calculated in the GCMC simulation) is plotted in comparison with the experimental values measured relative to the same reference. We see that in an absolute measure, the chemical shifts that we calculate are in rather good agreement with experiment.

One-body distribution functions are shown in Fig. 5 for Xe_1 in samples with various $\langle m\rangle_{Ar}$. These correspond to the probability of finding the center of a Xe atom within a voxel 0.307 Å on the side in the alpha cage. The one-body distribution function of xenon in the alpha cages containing Xe_1 is a good indicator of how the probability distribution of the Xe atoms in the alpha cage is affected by increasing the number of Ar atoms in the same cage with it. These probabilities become more localized (more sharply peaked) with increasing number of Ar atoms in the same cage with the xenon. As

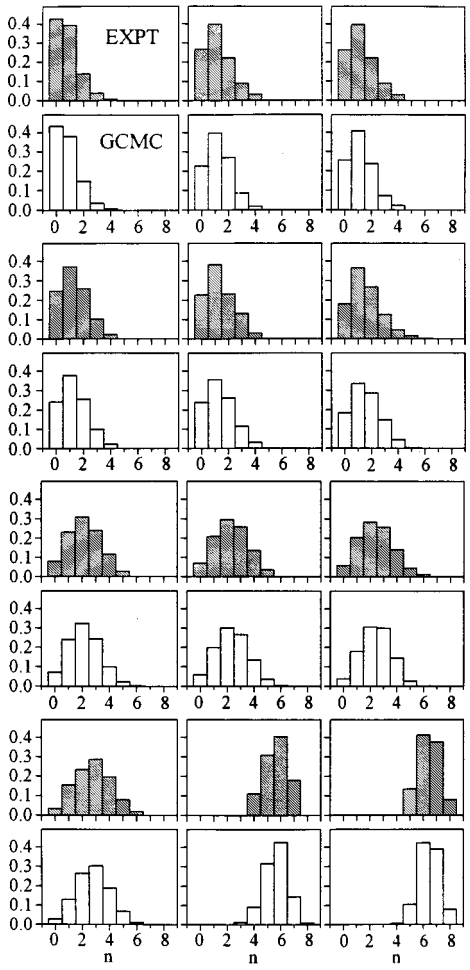

FIG. 2. The fractions of alpha cages containing n Xe atoms, P_n, from experiment and from GCMC simulations. The loadings are as follows: For the top row, $\langle n\rangle_{\mathrm{Xe}}=0.81$, $\langle m\rangle_{\mathrm{Ar}}=1.24$ (GCMC: $\langle n\rangle_{\mathrm{Xe}}=0.80$, $\langle m\rangle_{\mathrm{Ar}}=1.21$); 1.22, 3.60 (GCMC: 1.28, 3.53); 1.23, 4.79 (GCMC: 1.21, 4.88). For the second row: $\langle n\rangle_{\mathrm{Xe}}=1.28$, $\langle m\rangle_{\mathrm{Ar}}=2.14$ (GCMC: 1.29, 2.11); 1.36, 1.65 (GCMC: 1.34, 1.71); 1.54, 0.86 (GCMC: 1.55, 0.92). For the third row: $\langle n\rangle_{\mathrm{Xe}}=2.16$, $\langle m\rangle_{\mathrm{Ar}}=2.99$ (GCMC: 2.14, 3.05); 2.29, 1.15 (GCMC: 2.34, 1.20); 2.40, 3.09 (GCMC: 2.43, 3.14). For the bottom row: $\langle n\rangle_{\mathrm{Xe}}=2.77$, $\langle m\rangle_{\mathrm{Ar}}=1.85$ (GCMC: 2.75, 1.88); 5.65, 0.68 (GCMC: 5.63, 0.62); 6.40, 0.17 (GCMC: 6.42, 0.23).

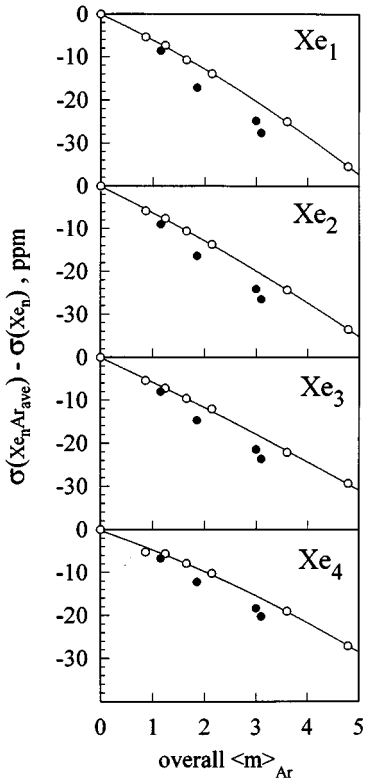

FIG. 3. Experimental ^{129}Xe chemical shifts of Xe_n, $\{\langle\sigma(\mathrm{Xe}_n\mathrm{Ar}_{\mathrm{ave}})\rangle-\langle\sigma(\mathrm{Xe}_n)\rangle\}$, for $n=1$ to 4 in mixtures of Xe and Ar in zeolite Na*A* for $\langle n\rangle_{\mathrm{Xe}}=0.81$–$1.54$ (○) and for $\langle n\rangle_{\mathrm{Xe}}=2.16$–$2.77$ (●). The curves are provided merely to guide the eye.

the overall $\langle m\rangle_{\mathrm{Ar}}$ is increased, every Xe_n suffers an increase in the average number of Ar atoms that coexist in the cage with it, but the average in specifically those cages containing only *one* Xe atom, $[\langle m\rangle_{\mathrm{Ar}}]_1$, changes over the widest range, as can be seen in Table III. As a consequence of this, what we see in Fig. 5 is that as the overall $\langle m\rangle_{\mathrm{Ar}}$ increases, the Xe density distribution becomes more sharply peaked at the adsorption sites. The Ar atoms occupy space within the alpha cage, limiting the volume available for the Xe atom. As the number of Ar atoms in the cage increases, the Xe atoms become more and more restricted to a smaller region of space, and since the Xe atoms are preferentially adsorbed over the Ar atoms, this space is preferentially near the adsorption sites. This is obvious in comparing Figs. 5(a) through 5(c).

Pair distribution functions $g[r(\mathrm{Xe}\text{–}\mathrm{Xe}]$ and $g[r(\mathrm{Xe}\text{–}\mathrm{Ar})]$ are shown in Fig. 6 for $\mathrm{Xe}_2\mathrm{Ar}_{4.254}$ and $\mathrm{Xe}_4\mathrm{Ar}_{2.068}$, as typical examples. These have been obtained specifically from those Xe atoms in Xe_n clusters with any number of Ar atoms in a loading such that there are an average number of 4.254 Ar atoms associated with Xe_2 and 2.068 Ar atoms with Xe_4. When there is at least one other Xe atom in the same alpha cage, the pair distribution functions provide good comparisons among the distribution of Xe–Xe, Xe–Ar, and Ar–Ar distances. We also obtained one-body distribution functions and overall pair distribution functions which are averages for the Xe–Ar mixture at the overall $\langle m\rangle_{\mathrm{Ar}}$ and $\langle n\rangle_{\mathrm{Xe}}$ associated with a given (μ_1,μ_2,T), but these are averages which are not nearly as informative as the examples in Fig. 5 and 6.

We also determined some minimum energy configurations for mixed clusters by methods described earlier.[43] Starting points for the determination of minimum energy configurations are collected during the GCMC runs by saving the lowest energy configuration of each mixed cluster found in the eight cages of the simulation box in each run. These provide a large number of independent starting configurations for steepest descent method or other methods of locating the closest local minimum. Some of the starting configurations descend into the same local minimum. For purposes of illustration we specifically collected configurations of two mixed clusters $\mathrm{Xe}_2\mathrm{Ar}_4$ and $\mathrm{Xe}_4\mathrm{Ar}_2$. The lowest energy configuration found for each are shown in Fig. 7. There are

TABLE III. Average number of Ar atoms in the same alpha cage with Xe_n, $[\langle m\rangle_{Ar}]_n$, for Xe–Ar mixtures in zeolite Na*A*.

Estimated from experiment									Overall	
Xe_0	Xe_1	Xe_2	Xe_3	Xe_4	Xe_5	Xe_6	Xe_7	Xe_8	$\langle m\rangle_{Ar}$	$\langle n\rangle_{Xe}$
0.98	0.92	0.86	0.67	0.52	0.30				0.86	1.54
1.33	1.22	1.12	0.89	0.56					1.24	0.81
1.99	1.75	1.51	1.17	0.79					1.65	1.36
2.58	2.25	1.93	1.44	1.02					2.14	1.28
4.28	3.74	3.20	2.48	1.83					3.60	1.22
5.80	5.00	4.19	3.18	2.49					4.79	1.23
1.55	1.43	1.30	0.99	0.67	0.38				1.15	2.29
3.19	2.73	2.26	1.73	1.20	0.69	0.40			1.85	2.77
4.28	3.73	3.18	2.42	1.76	1.10				2.99	2.16
4.71	4.08	3.44	2.63	1.94	1.22	0.67			3.09	2.40
				1.63	0.92	0.47	0.14		0.68	5.65
					0.50	0.20	0.07	0.00	0.17	6.40
GCMC results									Overall	
Xe_0	Xe_1	Xe_2	Xe_3	Xe_4	Xe_5	Xe_6	Xe_7	Xe_8	$\langle m\rangle_{Ar}$	$\langle n\rangle_{Xe}$
1.02	0.99	0.90	0.77	0.56	0.36				0.92	1.55
1.28	1.20	1.10	0.89	0.65					1.21	0.80
1.96	1.80	1.59	1.34	1.11	0.93				1.71	1.34
2.40	2.21	1.95	1.62	1.25	0.83				2.18	1.29
4.19	3.71	3.15	2.52	2.01	1.47				3.53	1.28
5.73	5.07	4.33	3.39	2.68	1.47				4.88	1.21
1.59	1.50	1.31	1.08	0.80	0.53	0.23			1.20	2.34
2.74	2.58	2.23	1.81	1.36	0.88	0.63			1.88	2.75
4.24	3.68	3.16	2.54	1.99	1.38	1.00			3.05	2.14
4.57	4.02	3.42	2.84	2.10	1.38	0.25			3.14	2.43
			1.54	1.21	0.87	0.43	0.22	0.06	0.62	5.63
				0.91	0.56	0.26	0.13	0.06	0.23	6.42
Hypergeometric model results									Overall	
Xe_0	Xe_1	Xe_2	Xe_3	Xe_4	Xe_5	Xe_6	Xe_7	Xe_8	$\langle m\rangle_{Ar}$	$\langle n\rangle_{Xe}$
1.061	0.9286	0.7960	0.6633	0.5307	0.3980	0.2653	0.1327	0.0000	0.86	1.54
1.379	1.206	1.035	0.8616	0.6893	0.5170	0.3446	0.1723	0.0000	1.24	0.81
1.983	1.735	1.487	1.239	0.9916	0.7437	0.4958	0.2479	0.0000	1.65	1.36
2.548	2.230	1.911	1.593	1.274	0.9556	0.6371	0.3185	0.0000	2.14	1.28
4.247	3.716	3.185	2.654	2.123	1.592	1.062	0.5308	0.0000	3.60	1.22
5.658	4.951	4.244	3.536	2.829	2.122	1.415	0.7073	0.0000	4.79	1.23
1.607	1.406	1.205	1.004	0.8035	0.6026	0.4018	0.2009	0.0000	1.15	2.29
2.824	2.471	2.118	1.765	1.412	1.059	0.7060	0.3530	0.0000	1.85	2.77
4.099	3.586	3.074	2.562	2.049	1.537	1.025	0.5123	0.0000	2.99	2.16
4.420	3.867	3.315	2.762	2.210	1.657	1.105	0.5525	0.0000	3.09	2.40
2.300	2.013	1.725	1.438	1.150	0.8626	0.5751	0.2875	0.0000	0.68	5.65
0.8600	0.7525	0.6450	0.5375	0.4300	0.3225	0.2150	0.1075	0.0000	0.17	6.40

many interesting aspects of the mixed cluster configurations.

First let us examine the relevant interatomic distances. These are shown in Table IV with the r_{min} of the pair interaction potential for comparison. The lowest energy configuration found for Xe_2Ar_4 has the characteristic distances (Structure I) shown in Table IV, although other distinct configurations were found, one only 119 J mol^{-1} above this (Structure II). Similarly, the lowest energy configuration found for Xe_4Ar_2 has the characteristic distances shown (Structure II) but there are several other configurations only 14–90 J mol^{-1} above this one which has only very slightly different distances (a typical one is Structure I) shown in Table IV. Just as was found for the pure Xe_n clusters, there are usually several nearly equivalent configurations which differ only in their orientation relative to the alpha cage, but which maintain the same or very nearly the same Xe–Xe, Xe–Ar, and Ar–Ar distances.

Let us first consider the mixed cluster Xe_2Ar_4. The Xe–Xe distance at 5.03 Å is longer than the typical nearest Xe–Xe distances in the pure Xe_n clusters in zeolite Na*A* at their minimum energy configurations, 4.2 and 4.7 Å for Xe_2, for example.[43] We had found earlier that the distances between the 11 adsorption sites (3.6, 5.1, 6.2, and 7.2 Å) make it energetically unfavorable for two Xe atoms to be in register with the Xe–zeolite potential minima and simultaneously be 3.6 Å apart. The large Xe–Xe repulsive energies at such close separations is relieved by a compromise arrangement in which the Xe–Xe distance is within the r_{min} of the Xe_2

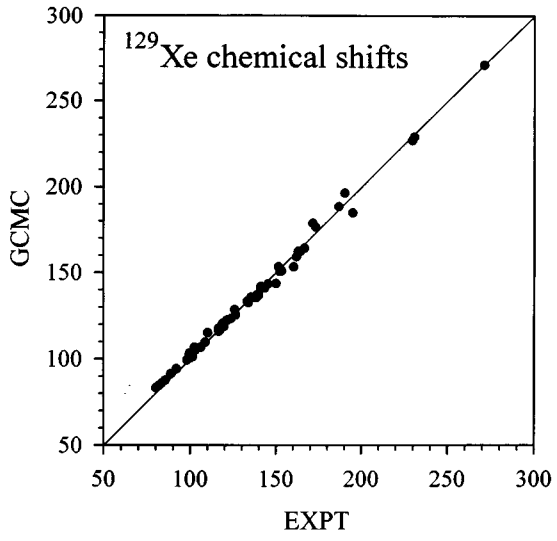

FIG. 4. The ^{129}Xe chemical shifts of Xe_n in Ar under fast exchange in zeolite Na*A*, obtained from GCMC simulations compared with experimental values. The shifts are relative to the isolated Xe atom.

potential function while each Xe is still within an rms distance of 0.2 Å of one of the 11 adsorption sites of a single Xe atom in the alpha cage. In the mixed cluster Xe_2Ar_4, on the other hand, the distances between the Xe atoms and the closest adsorption site are 0.001 and 0.003 Å, much shorter than any of the typical Xe-to-adsorption site distances at the minimum energy configurations of various Xe_n in the absence of Ar.[43] The Xe in the mixed clusters have the opportunity to sit much closer to the adsorption site of a single Xe atom in the alpha cage than they do in the pure Xe_n clusters. In both Xe_2Ar_4 and Xe_4Ar_2 the Ar atoms are found 0.019–0.048 Å from the adsorption sites of a single Ar atom in Na*A*. In Xe_2Ar_4, each Xe and Ar atom is closer to its adsorption sites than either Xe or Ar in the pure clusters Xe_n and Ar_m. Structure I has six short (3.93–3.97 Å) and two long (6.60–6.61 Å) Xe–Ar distances while Structure II has four short and four long distances in the same ranges. To accompany these, Structure I has two short and four long Ar–Ar distances, Structure II has four short and two long distances. Nevertheless, all low energy configurations of mixed clusters Xe_2Ar_4

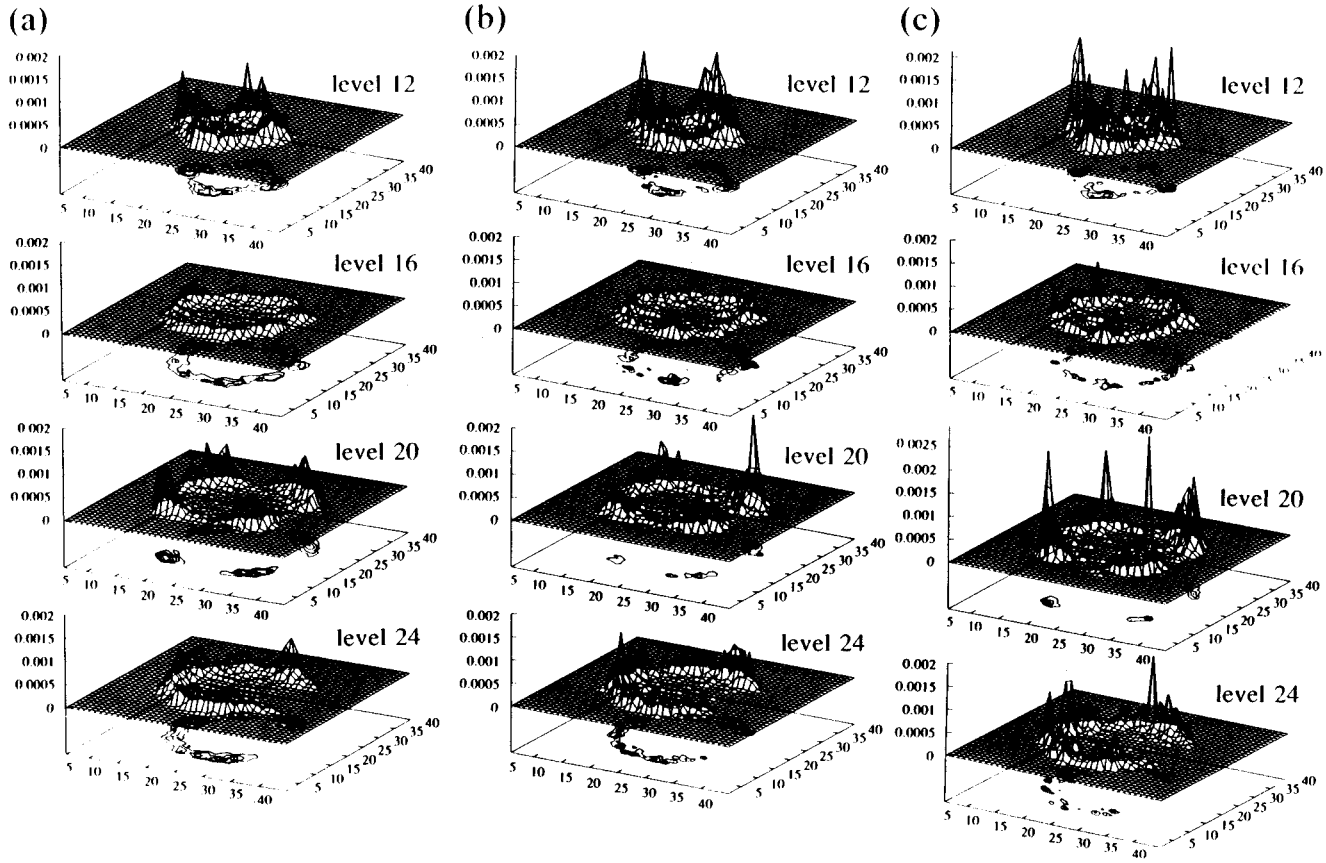

FIG. 5. Normalized one-body distribution functions for Xe_1 in cages having (a) $\langle m\rangle_{Ar}=0.73$, (b) $\langle m\rangle_{Ar}=3.33$, (c) $\langle m\rangle_{Ar}=5.07$ at 300 K. The slices at levels 12, 16, 20, and 24 of the $40\times40\times40$ stored distributions correspond to planes at $z=3.7365$ Å, $z=4.982$ Å, $z=6.2275$ Å, $z=7.473$ Å of the pseudo unit cell which is 12.2775 Å on a side. The asymmetry of the picture in level 24 is due to the location of Na(III) inside the cage.

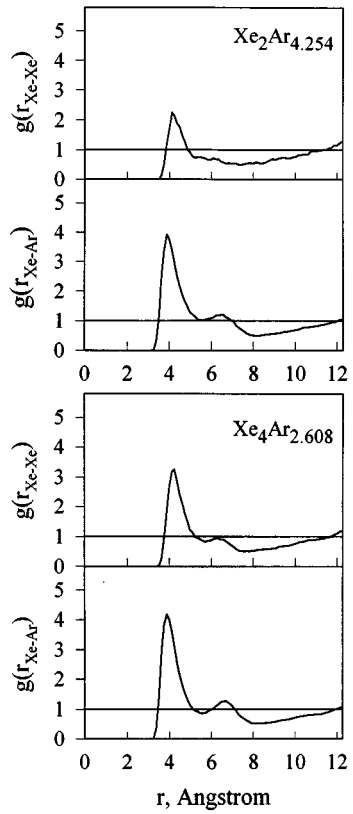

FIG. 6. Pair distribution functions in an alpha cage containing $Xe_2Ar_{4.254}$ and $Xe_4Ar_{2.068}$. The average number of Ar atoms accompanying Xe_2 and Xe_4 are as indicated.

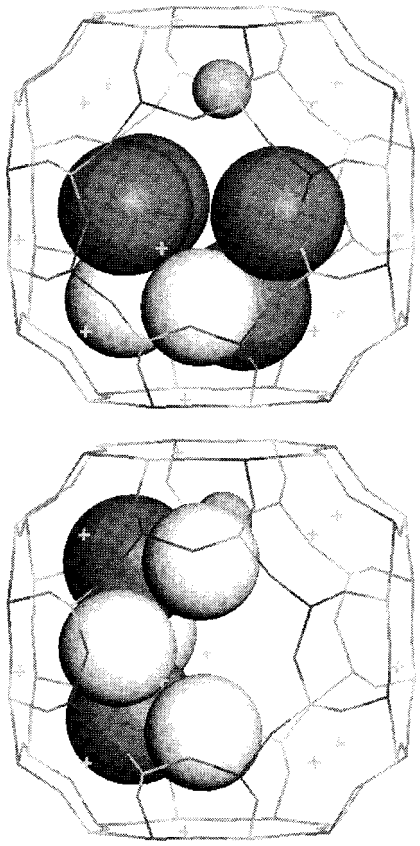

FIG. 7. Minimum energy configurations for the mixed clusters Xe_2Ar_4 and Xe_4Ar_2.

are found to be close to the wall of the zeolite cage, as seen in the example in Fig. 7.

Let us now consider the mixed cluster Xe_4Ar_2. There are several equivalent configurations (Structure I) which differ only in their orientation with respect to the alpha cage and have essentially identical interatomic distances. There are four favorably short Xe–Xe distances (4.2–4.6 Å), five short Xe–Ar distances (3.93–3.98 Å), but an unusually long Ar–Ar distance (7.2 Å). Another configuration with nearly identical energy (Structure II) has three Xe–Xe distances in the range 4.8–5.0 Å, six favorably short Xe–Ar distances (3.9–4.1 Å) and a favorable Ar–Ar distance (3.81 Å). This structure has three Xe atoms very close to the adsorption sites but one is an unusually large distance away (2.83 Å).

The minimum energy structures for selected mixed clusters in Fig. 7 agree with what we see in the average one-body and pair distribution functions at 300 K, as shown in Figs. 5 and 6. As we have seen already, in the example of Structures I and II of the Xe_4Ar_2 cluster, there are many local minima in the potential surface of a mixed cluster with different combinations of Xe–Xe, Xe–Ar and Ar–Ar distances. The average pair distribution functions at 300 K, such as those seen in Fig. 6 reflect the average over three million configurations out of which we have selected the ones having Xe_2 and Xe_4 only, and the average number of Ar atoms in the same alpha cage are respectively 4.254 and 2.086. The Xe–Xe distance in the minimum energy configuration of Xe_2Ar_4 (5.0 Å) and the short Xe–Xe distances in the minimum energy configuration of Xe_4Ar_2 (4.8–5.2, 6.1 Å), are somewhat longer than the position of the first maximum (at ca. 4.2 Å) in the $g[r(\mathrm{Xe–Xe})]$ of $Xe_2Ar_{4.254}$ at 300 K shown in Fig. 6. The next nearest Xe–Xe distances in the Xe_4Ar_2 minimum energy configuration are close to the second maximum at 6.3 Å in the $g[r(\mathrm{Xe–Xe})]$ of $Xe_4Ar_{2.068}$ at 300 K. The Xe–Ar distances in Xe_2Ar_4 (3.9 and 6.6 Å) are close to the positions of the maxima at 3.8 and 6.5 Å in the $g[r(\mathrm{Xe–Ar})]$ of $Xe_2Ar_{4.254}$ at 300 K shown in Fig. 6. The Ar–Ar distances in the minimum energy configuration of Xe_2Ar_4 (3.9–4.0, 5.5–6.1 Å) are likewise close to the positions of the maxima in the typical $g[r(\mathrm{Ar–Ar})]$ of the mixture at 300 K (not shown). Although we have not presented a minimum energy configuration for each of the mixed clusters observed in the alpha cages during the GCMC simulation, the typical configurations have interatomic distances that are reflected in the pair distribution functions and the one-body distribution functions used as examples in Figs. 5 and 6. These molecular-level details provide the background in which the average ^{129}Xe chemical shifts observed for the Xe_n peaks under various Xe and Ar loadings in Na*A* may be understood.

Of interest also are the much lower energies associated with the Xe_4Ar_2 cluster in the zeolite cage (-126.5 kJ mol^{-1}) than for the complementary 6-particle cluster Xe_2Ar_4 (-105.4 kJ mol^{-1}). We shall see later that there are

TABLE IV. Distances in the minimum energy configurations of two mixed clusters, Å.

		Xe_2Ar_4				Xe_4Ar_2			
		Structure I		Structure II		Structure I		Structure II	
Pair	r_{min} of pair	Nearest	Next nearest	Nearest	Next nearest	Nearest	Next nearest	Nearest	Next nearest
Xe–Xe	4.363	5.03		4.82		4.25–4.59	6.2–6.3	4.8–5.2	6.1–7.1
Xe–Ar	4.067	3.91–3.97	6.60	3.98–4.05	6.56–6.64	3.93–3.98	5.7–7.6	3.94–4.10	6.50–6.55
Ar–Ar	3.761	3.88–3.90	5.5–7.2	3.86–3.90	5.44–5.53	7.17		3.81	
Xe site[a]	0.0	0.001	0.003	0.029	0.036	0.045–0.047	0.36–0.47	0.003–0.035	2.83
Ar site[a]	0.0	0.019–0.020	0.040–0.048	0.019–0.025	0.056	0.003	0.020	0.012	0.047

[a]Distance of Xe or Ar in the mixed cluster to the minimum energy sites for an single Xe or Ar in Na*A*.

important consequences of these not unexpected GCMC results which are manifested in the experimentally observed distribution and ^{129}Xe chemical shifts in the coadsorbed system in Na*A*.

DISCUSSIONS

The statistical (hypergeometric) distribution of a binary mixture of distinguishable but equivalent atoms

A simple model for the distribution of molecules in the cages of a zeolite is the hypergeometric distribution.[44] By assuming that molecules occupy K mutually exclusive lattice sites in the subvolume (alpha cage), for N molecules in a volume V, the probability H_i that any subvolume contains i molecules has been derived,[45]

$$H_i=\frac{\binom{N}{i}\binom{M-N}{K-i}}{\binom{M}{K}},$$

where M is the number of subvolumes in the volume V and

$$\binom{M}{K}=\frac{M!}{K!(M-K)!}.$$

In the limit where the number of subvolumes and N are very large, it can be shown that the above expression approaches the limiting form,[5]

$$H_i=\langle i\rangle^i(K-\langle i\rangle)^{(K-i)}K!/K^K i!(K-i)!,$$

where $\langle i\rangle=N/M=$the average number of molecules per subvolume. In the case of xenon in the alpha cages of zeolite Na*A*, it can be assumed that $K=8$ is a reasonable model since the Xe_8 cluster has been observed but not Xe_9.

We can derive a simple model for binary mixtures in which the two components are distinguishable but equivalent, that is, they compete equally for the same lattice sites under the rule of mutual exclusion. We consider blue and red particles in a binary mixture containing an average number, $\langle n\rangle$, blue particles per alpha cage and an average number, $\langle m\rangle$, red particles per alpha cage. The intrinsic probability of finding a blue particle is $\langle n\rangle/(\langle n\rangle+\langle m\rangle)$ and the number of ways of arranging n blues and m reds is $(n+m)!/n!m!$ Thus, the fraction, $f(n,m)$, of alpha cages containing specifically n blues and m reds is simply related to the fractions H_i where $i=n+m$, that is,

$$f(n,m)=\frac{H_i\langle n\rangle^n\langle m\rangle^m}{n!m!\sum_{k=0}^{n}[\langle n\rangle^k\langle m\rangle^{i-k}/k!(i-k)!]},$$

where, H_i is the fraction of cages having i particles regardless of color, given by the equation above. Supposing that only blue particles can be observed, we wish to know the fraction, P_n, of cages containing specifically n blue particles, regardless of the number of red particles with it, which is given by,

$$P_n=\sum_{m=0} f(n,m),$$

just as in the realistic case. In this simple model, it is trivial to calculate $f(n,m)$ for any average occupancies $\langle n\rangle$ and $\langle m\rangle$. This simple model is a limiting statistical case for coadsorption which strictly applies only when the two sorbates are equivalent in the hypergeometric distribution, for example two different isotopes such as ^{131}Xe and ^{129}Xe. For Xe and Ar in an alpha cage of zeolite Na*A*, there are different numbers of maximum occupancies for Xe and Ar, 8 for Xe and probably 11 for Ar, so this statistical model is not valid. Nevertheless, it serves as a means of gaining insight into the complex problem of detailed distributions of adsorbates in competitive adsorption and also provides a limiting case with which we may compare the more realistic GCMC simulations. For example, with the $f(n,m)$ estimated from the model hypergeometric distribution for a sample of arbitrary loading of Xe and Ar, the average properties of the system can be calculated. The similarities in trends (with loading) between the GCMC and the hypergeometric distribution based on the strictly statistical ideal mixture can be attributed to the properties of the latter, whereas the differences between their trends can be attributed to the non-ideal nature of the mixed adsorbates. For example, Fig. 8 shows the dependence of $f(n,m)$ on n and m for selected values of $\langle n\rangle$ and $\langle m\rangle$, compared with the results of GCMC simulations for the same overall $\langle n\rangle$ and $\langle m\rangle$.

We have already mentioned that the ^{129}Xe chemical shift observed for the cages containing n Xe atoms in the samples of adsorbed Xe–Ar mixtures relative to that in the adsorbed pure xenon samples is determined entirely by the average

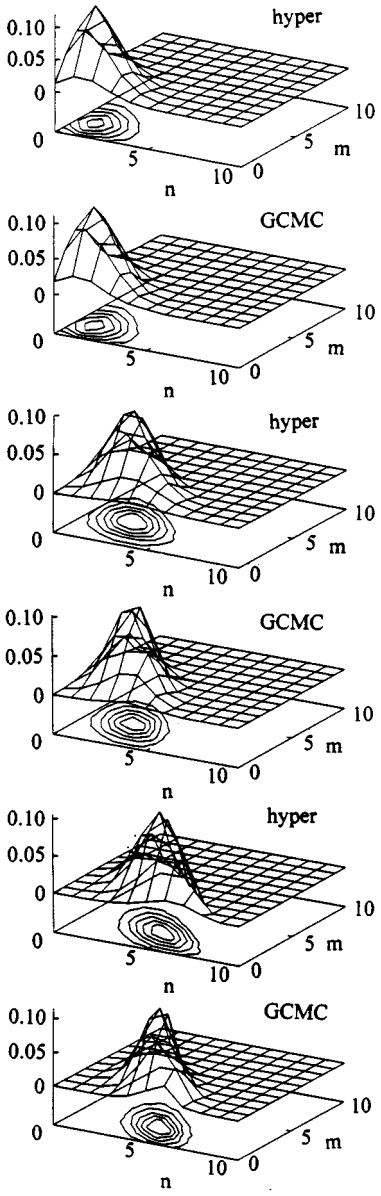

FIG. 8. The distribution $f(n,m)$ as a function of (n,m), for $\langle n\rangle_{\mathrm{Xe}}=1.23$, $\langle m\rangle_{\mathrm{Ar}}=2.08$ (top), $\langle n\rangle_{\mathrm{Xe}}=2.43$, $\langle m\rangle_{\mathrm{Ar}}=3.14$ (middle), and $\langle n\rangle_{\mathrm{Xe}}=4.19$, $\langle m\rangle_{\mathrm{Ar}}=2.46$ (bottom) calculated from the hypergeometric distribution and from GCMC simulations.

$[\langle m\rangle_{\mathrm{Ar}}]_n$ for those cages. Therefore, let us examine $[\langle m\rangle_{\mathrm{Ar}}]_n$ using the strictly statistical hypergeometric distribution of distinguishable equivalent components. We find the expected trends: First of all, for a given sample, $[\langle m\rangle_{\mathrm{Ar}}]_n$ decreases with increasing n. That is, the largest $[\langle m\rangle_{\mathrm{Ar}}]_n$ is for those cages containing no Xe atoms, and the smallest is for those cages containing 7 Xe atoms. Of course, $[\langle m\rangle_{\mathrm{Ar}}]_n$ is exactly zero for those cages containing 8 Xe atoms, since we assume only 8 lattice sites. This trend is easily explained: for a given sample, there is a given number of Xe atoms and Ar atoms to be distributed among the cages; those cages with fewer Xe atoms have more sites for Ar atoms than the cages occupied by a larger number of Xe atoms. A second trend is observed in comparing several samples, for a given $\langle n\rangle_{\mathrm{Xe}}$, increasing the overall $\langle m\rangle_{\mathrm{Ar}}$ leads to larger $[\langle m\rangle_{\mathrm{Ar}}]_n$ for each Xe_n. This is what we may call the primary effect. In the examples shown in Table V, calculated for the ideal mixture model of distinguishable but equivalent blue (representing Xe atoms) and red atoms (representing Ar), the average $[\langle m\rangle_{\mathrm{Ar}}]_n$ for those cavities containing a particular number of Xe, say Xe_2, is increasing in the following order: 0.857, 1.71, 2.57, 3.43, 4.29 as the overall $\langle m\rangle_{\mathrm{Ar}}$ varies from 1.0 to 5.0. This trend holds for every cluster. This comes about naturally from the fixed total number of Xe atoms distributed into the cages, leaving a fixed number of sites into which the increasing total number of the Ar atoms have to distribute themselves.

A third trend is an increase in the $[\langle m\rangle_{\mathrm{Ar}}]_n$ for those cavities containing a particular number of Xe atoms, as the overall $\langle n\rangle_{\mathrm{Xe}}$ increases while keeping the overall $\langle m\rangle_{\mathrm{Ar}}$ the same for all samples. We may call this a secondary effect. As the $\langle n\rangle_{\mathrm{Xe}}$ increases, there is an increase in the $[\langle m\rangle_{\mathrm{Ar}}]_n$ for *every* Xe_n. For example, in Table V, for Xe_2, the $[\langle m\rangle_{\mathrm{Ar}}]_2$ is increasing in the following order: 0.857, 1.00, 1.20, 1.50, 2.0 as $\langle n\rangle_{\mathrm{Xe}}$ varies from 1.0 to 5.0. This trend holds for every cluster. The explanation for this trend is somewhat less obvious. Consider a fixed number of Ar atoms to distribute among a fixed number of cages. At low $\langle n\rangle_{\mathrm{Xe}}$, the Ar atoms are distributed among cages having few Xe atoms, so $[\langle m\rangle_{\mathrm{Ar}}]_n$ is relatively low for all n. At high loading of Xe, the same fixed number of Ar atoms will be distributed among cages containing many Xe atoms and there are virtually no cages containing 0, 1, or 2 Xe atoms; that is, the probability

TABLE V. Distributions in an ideal mixture of distinguishable equivalent particles competing for eight lattice sites under mutual exclusion.

Overall $\langle n\rangle_{\mathrm{blue}}$	Overall $\langle m\rangle_{\mathrm{red}}$	Average number of red atoms in a subvolume with n blue atoms, $[\langle m\rangle_{\mathrm{red}}]_n$								
		$n=0$	1	2	3	4	5	6	7	8
1.0	1.0	1.143	1.0	0.8571	0.7143	0.5714	0.4286	0.2857	0.1429	0
1.0	2.0	2.286	2.0	1.714	1.429	1.143	0.8571	0.5714	0.2857	0
1.0	3.0	3.429	3.0	2.571	2.149	1.714	1.286	0.8571	0.4286	0
1.0	4.0	4.571	4.0	3.429	2.857	2.286	1.714	1.143	0.5714	0
1.0	5.0	5.714	5.0	4.286	3.571	2.857	2.143	1.429	0.7143	0
2.0	1.0	1.333	1.167	1.0	0.8333	0.6667	0.5	0.3333	0.1667	0
3.0	1.0	1.6	1.4	1.2	1.0	0.8	0.6	0.4	0.2	0
4.0	1.0	2.0	1.75	1.5	1.25	1.0	0.75	0.5	0.25	0
5.0	1.0	2.667	2.333	2.0	1.667	1.333	1.0	0.6667	0.3333	0

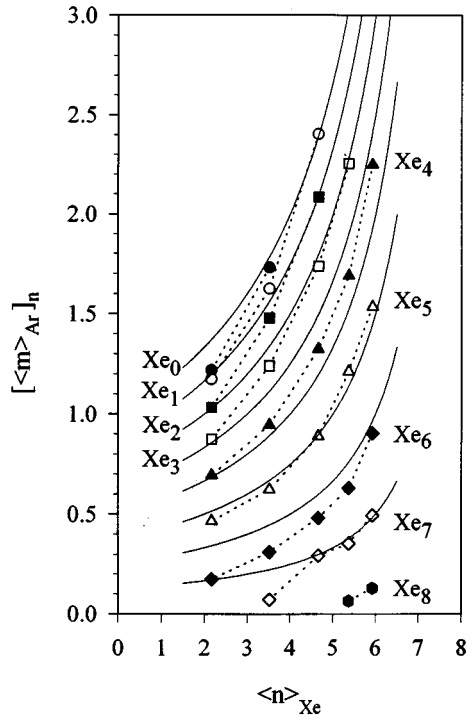

FIG. 9. The solid curves are the average number of Ar atoms in the same cage as the Xe_n cluster, $[\langle m\rangle_{Ar}]_n$ vs overall $\langle n\rangle_{Xe}$ for fixed overall $\langle m\rangle_{Ar}=1.00$, calculated from the hypergeometric distribution. The points are the average number of Ar atoms in the same cage as the Xe_n cluster, $[\langle m\rangle_{Ar}]_n$ vs overall $\langle n\rangle_{Xe}$ for almost identical overall $\langle m\rangle_{Ar}$ (0.986–1.013), calculated from GCMC simulations.

of the various cage types at high loading of Xe is radically different from the low Xe loading case. As the $\langle n\rangle_{Xe}$ varies from 1.0 to 7.0 the total number of sites available for the fixed total number of Ar atoms decreases as the sites are taken up by Xe atoms which are increasing in total number. The consequence is that the $[\langle m\rangle_{Ar}]_n$ for each Xe_n cluster goes up. This secondary effect is clearly shown by the solid curves in Fig. 9 where a fourth related trend is also observed: the increase in the $[\langle m\rangle_{Ar}]_n$ for a given Xe_n cluster as the overall $\langle n\rangle_{Xe}$ increases, while keeping the overall $\langle m\rangle_{Ar}$ the same, is less and less pronounced with increasing n. All these trends are derived from the simple model using the strictly statistical hypergeometric distribution of distinguishable equivalent components. We expect to see these trends also in the real situation where the Xe and Ar are no longer equivalent particles as they are in this model. (See below under Deviations From Ideal Mixtures.)

Since the ^{129}Xe chemical shift of the Xe_n with some average number of Ar atoms depends on the average number of Ar atoms in the cage with it, the larger the $[\langle m\rangle_{Ar}]_n$ for that particular Xe_n the larger the chemical shift relative to the Xe_n in the pure xenon in Na*A*. Let us see what the strictly statistical model gives us: In Table V we have a model for the average $[\langle m\rangle_{Ar}]_n$ for only those cages containing specifically n Xe atoms while keeping the overall $\langle m\rangle_{Ar}$ the same for all samples. This model also leads to the prediction that when $\langle n\rangle_{Xe}$ is approximately the same in several samples, ^{129}Xe chemical shift of the Xe_n will become larger as the overall $\langle m\rangle_{Ar}$ is increased. This trend is indeed observed experimentally. It has to do with the general increase in the $[\langle m\rangle_{Ar}]_n$ for each Xe_n that we have illustrated in Fig. 9. How much the Xe_n chemical shift increases with an increase in the overall $\langle m\rangle_{Ar}$ is almost predictable from the gas phase density dependence of chemical shifts due to Xe–Ar interactions compared to Xe–Xe,[28] and the known incremental chemical shift upon increasing the cluster size in the Xe/Na*A* system.[5] Thus the Xe_n chemical shift in a sample of Xe–Ar in Na*A* is expected to have a primary dependence on the overall $\langle m\rangle_{Ar}$. Furthermore, there will be a secondary dependence on the overall $\langle n\rangle_{Xe}$: Since we have already seen in Fig. 9 the increase in the $[\langle m\rangle_{Ar}]_n$ for each Xe_n as the overall $\langle n\rangle_{Xe}$ increases while the overall $\langle m\rangle_{Ar}$ remains fixed, we expect for strictly statistical reasons to find the individual Xe_n chemical shifts relative to the Xe_n in pure Xe in Na*A* to increase with increasing overall $\langle n\rangle_{Xe}$ at fixed overall $\langle m\rangle_{Ar}$. Therefore, the solid curves in Fig. 9, derived from a simple statistical model, explains in very plain terms why the individual Xe_n chemical shifts should vary primarily with overall $\langle m\rangle_{Ar}$ and secondarily with overall $\langle n\rangle_{Xe}$, just as observed experimentally. The qualitative trends in the chemical shifts are observed experimentally just as expected from the predictions of a simple model of distinguishable particles which compete equally for the same lattice sites. The larger number of sites per cavity for the Ar atoms and the weaker interactions between the Ar–Ar compared to the Xe–Xe and Xe–Ar, and the different adsorption energies of Xe and Ar have not been taken into account. Quantitative predictions will require a more realistic model, such as the GCMC simulations. However, the strictly statistical results offer considerable insight even at this crude level.

Comparison of the GCMC Xe–Ar distribution with experiment

In Table I and Fig. 2 we show a comparison of the experimental P_n with the P_n obtained from GCMC simulations of Xe–Ar mixtures at close to the experimental values of overall $\langle n\rangle_{Xe}$ and overall $\langle m\rangle_{Ar}$. The simulations quantitatively reproduce the experimental observations for all 12 samples. Another important comparison with experiment is the $[\langle m\rangle_{Ar}]_n$ associated with each Xe_n, which determines the ^{129}Xe chemical shift observed for Xe_n with Ar under fast exchange in a given sample. The values obtained from the GCMC simulation are compared in Table III with those estimated from the experimental chemical shifts as described earlier. We find the agreement is quite reasonable, given the approximations associated with the estimates.

How well does the simple model of distinguishable equivalent particles do in comparison with experimental estimates or the results of the GCMC simulations? The values predicted by the hypergeometric model are also shown in Table III. It is even more enlightening to compare the ideal mixtures with the same overall $\langle m\rangle_{red}=1.0$ and various $\langle n\rangle_{blue}$ (shown in Fig. 9 as solid curves) with the GCMC (results shown as points) for almost the same overall $\langle m\rangle_{Ar}$

(0.986–1.013) and various $\langle n\rangle_{\mathrm{Xe}}$. The trends are qualitatively the same which emphasizes the usefulness of a simple model. For this low loading of coadsorbate, the simple model should do very well since at low numbers of Ar the difference in size between the Xe and the Ar does not significantly affect the distribution of Ar atoms among the cages containing Xe atoms. At much higher loading the discrepancies could be more pronounced. At low overall Ar loading (overall $\langle m\rangle_{\mathrm{Ar}}\cong 1.0$), for the exactly same Xe and Ar loading, the more realistic GCMC model shows that, the ideal hypergeometric mixture predicts too low values of $[\langle m\rangle_{\mathrm{Ar}}]_n$ for cages containing Xe_2, Xe_3, Xe_4, and Xe_8, too high $[\langle m\rangle_{\mathrm{Ar}}]_n$ values for cages containing no Xe atoms, Xe_6 and Xe_7, and a crossover from too high to too low $[\langle m\rangle_{\mathrm{Ar}}]_n$ with increasing $\langle n\rangle_{\mathrm{Xe}}$ for cages containing Xe_1 and Xe_5. These differences between GCMC results and hypergeometric results for exactly the same overall values of $\langle m\rangle_{\mathrm{Ar}}$ and $\langle n\rangle_{\mathrm{Xe}}$ are due to such complexities of the real system as the different pair potentials for Xe–Xe, Xe–Ar, and Ar–Ar, the mutual exclusion not necessarily being associated with a fixed number of lattice sites, and the maximum number of particles that can be accommodated in an alpha cage being variable in the real system, depending on the kinds of particles. The subtle differences of up to about 0.3 Ar atoms in a cage compared to the strictly statistical distribution are due specifically to these factors. Nevertheless, the observed qualitative trends in the variation of the Ar occupancies accompanying different Xe_n clusters are just as predicted by the ideal mixture model and are therefore shown to be strictly statistical in origin.

Comparison of GCMC simulations of the average ^{129}Xe chemical shifts in Xe_n clusters with Ar under fast exchange with experiment

One of the interesting experimental observations in Table II is that the larger the Xe_n cluster the smaller the dependence of the ^{129}Xe chemical shift on the overall $\langle m\rangle_{\mathrm{Ar}}$. This is observed despite the fact that the larger Xe_n clusters have larger incremental shifts. The explanation for this is an obvious one: Xe_1 can have any number from 1 to 9 Ar atoms with it in the cage, and the Xe_1 chemical shift can thus vary over a wide range, according to the $[\langle m\rangle_{\mathrm{Ar}}]_1$ for the cages containing only one Xe atom, as the overall $\langle m\rangle_{\mathrm{Ar}}$ is varied. On the other hand Xe_7 can have at most 1 or 2 Ar atoms with it in the cage, no matter how much the overall $\langle m\rangle_{\mathrm{Ar}}$ is increased. Now let us see how well the GCMC simulations predict the observed ^{129}Xe chemical shifts in the mixture compared to that in the pure Xe in Na*A*. In Fig. 4 we compare the experimental Xe_n cluster chemical shifts in 12 different samples of Xe–Ar mixtures in Na*A* with the GCMC simulations of the average chemical shifts in Xe–Ar systems with close to the same values of overall $\langle n\rangle_{\mathrm{Xe}}$ and overall $\langle m\rangle_{\mathrm{Ar}}$ as the twelve samples. The agreement with experiment is reasonably good. These chemical shifts are measured relative to an isolated Xe atom and are therefore a measure of the total intermolecular shielding. The shielding difference between Xe_n with Ar under fast exchange and Xe_n alone is a more stringent test. On an individual one-to-one comparison in Table II, these simulated shielding differences are in quantitative agreement with experiment. The trends with increasing overall $\langle m\rangle_{\mathrm{Ar}}$ of the shielding differences $\{\langle\sigma(\mathrm{Xe}_n\mathrm{Ar}_{\mathrm{ave}})\rangle-\langle\sigma(\mathrm{Xe}_n)\rangle\}$ for samples with overall $\langle n\rangle_{\mathrm{Xe}}$ close to 1, those for overall $\langle n\rangle_{\mathrm{Xe}}$ close to 2, and those whose Xe loadings are higher yet, are preserved, especially for the smaller clusters.

Let us now consider the ^{129}Xe chemical shifts in the Xe–Ar mixture compared to that in the pure Xe in Na*A* using the $f(n,m)$ from the hypergeometric distribution to calculate the average Xe shielding under fast exchange of Ar by the equation,

$$\langle\sigma(\mathrm{Xe}_n\mathrm{Ar}_{\langle m\rangle})\rangle=\sum_{m=0}\sigma(\mathrm{Xe}_n\mathrm{Ar}_m)f(n,m)_{\langle n\rangle,\langle m\rangle}\Big/\sum_{m=0}f(n,m)_{\langle n\rangle,\langle m\rangle}$$

and compare the quantity on the left side of the equation with what we observe experimentally. The average shielding of a mixed cluster $\sigma(\mathrm{Xe}_n\mathrm{Ar}_m)$ is taken from the GCMC simulations. In Table II, we see that the simple model already gives rough agreement with experimental chemical shifts, especially for the lower Xe loadings, when the average ^{129}Xe shieldings for the individual mixed clusters $\mathrm{Xe}_n\mathrm{Ar}_m$ in a cage are used with the $f(n,m)$ from the simple model. The simple model does not do as well for the higher Xe clusters, the chemical shifts for these in the simple model are too large since the model predicts $[\langle m\rangle_{\mathrm{Ar}}]_n$ for each Xe_n that are too large. Upon close examination of Table II we find the magnitude of $\{\langle\sigma(\mathrm{Xe}_n\mathrm{Ar}_{\langle m\rangle})\rangle_{\mathrm{hyp}}-\langle\sigma(\mathrm{Xe}_n)\rangle\}$ is somewhat larger than experiment. The discrepancy relative to experiment generally increases with increasing n in the same sample and is generally worse for larger $[\langle m\rangle_{\mathrm{Ar}}]_n$ and for larger overall $\langle n\rangle_{\mathrm{Xe}}$.

To investigate the strictly statistical components of the observed changes in the Xe_n chemical shifts, we make in Fig. 10 a plot of the chemical shifts for the Xe_n clusters calculated for the ideal mixture having the hypergeometric distribution as a function of overall $\langle m\rangle_{\mathrm{Ar}}$, analogous to the experimental plot in Fig. 3, except that, for clarity in Fig. 10 we use two values of overall Xe loading which are the averages of the experimental ones: $\langle n\rangle_{\mathrm{Xe}}=1.25$ and 2.40, whereas Fig. 3 reflects the actual experimental Xe loadings: $\langle n\rangle_{\mathrm{Xe}}=(0.81–1.54)$ and (2.16–2.77). In calculating the Xe_n chemical shifts by the above equation, only the distribution, that is the $f(n,m)$ values, have been taken from the simple model; the average chemical shifts of the individual $\mathrm{Xe}_n\mathrm{Ar}_m$ mixed clusters are taken from the averages accumulated during the GCMC simulations. The primary effect on the chemical shift in mixtures of xenon and argon is clearly seen in the curves in Fig. 10: The chemical shift of each cluster increases with increasing overall $\langle m\rangle_{\mathrm{Ar}}$ due to the general increase in the average number of Ar atoms residing with a cluster of a given size, as the total number of argon atoms in the zeolite sample increases. In addition, the averages $\langle\sigma(\mathrm{Xe}_n\mathrm{Ar}_{\langle m\rangle})\rangle$ calculated in the ideal hypergeometric mixture model for a fixed $\langle m\rangle_{\mathrm{Ar}}$ with a varying $\langle n\rangle_{\mathrm{Xe}}$ show the sec-

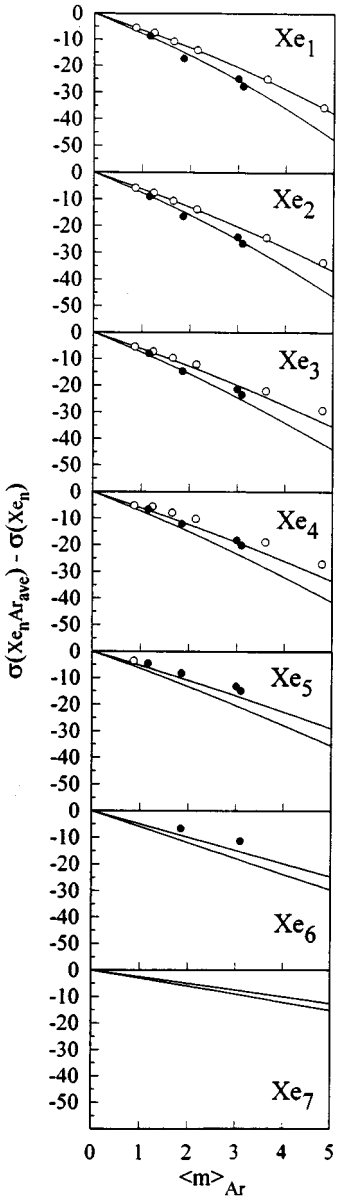

FIG. 10. The average Xe_n chemical shifts in mixtures of Xe and Ar in zeolite Na*A*, as predicted by the hypergeometric distribution for $\langle n\rangle_{Xe}=1.25$ and 2.40 are shown as curves. Superimposed are the values from experiment at $\langle n\rangle_{Xe}=0.81-1.54$ (○) and for $\langle n\rangle_{Xe}=2.16-2.77$ (●).

ondary effects of $\langle n\rangle_{Xe}$ on the individual cluster shifts. The predicted curve corresponding to the higher $\langle n\rangle_{Xe}$ (2.40) falls *below* the curve corresponding to $\langle n\rangle_{Xe}=1.25$ for each Xe_n. This observed dependence of the Xe_n cluster shifts on the Xe loading in the Xe–Ar mixture, in contrast to the invariance of the Xe_n cluster shifts with the Xe loading in pure Xe, is a property of the ideal mixture, so its occurrence is strictly a statistical phenomenon, not a result of the differences between Xe and Ar, or their interactions with each other, or with their different interactions with the zeolite cage. Indeed, when we superimpose the values from experiment onto the ideal hypergeometric mixture curves in Fig. 10, we see that the qualitative features of the experimental data are very similar to the ideal mixture curves, which further supports the usefulness of having a simple model. At the same values of $\langle n\rangle_{Xe}=1.25$, the Xe_n chemical shifts in the presence of Ar in fast exchange relative to the Xe_n chemical shifts in the absence of a second component vary with the overall $\langle m\rangle_{Ar}$ in our simple model, just as in the GCMC simulations, and just as in experiments in Fig. 3, although the wider spread of the $\langle n\rangle_{Xe}=0.81-1.54$ for the experimental data leads to a somewhat greater scatter. The hypergeometric model shows non-linear change in the chemical shifts of the individual Xe_n as the overall $\langle m\rangle_{Ar}$ increases, and the curvature becomes less pronounced as n increases. This has to do with the nonlinear change in the chemical shifts of ^{129}Xe in the mixed clusters Xe_nAr_m with the addition of Ar atoms. For Xe_1 and Xe_2, the experimental points do fall reasonably close to the curves for the idealized model. The slopes of the experimental data systematically become less steep as the cluster size n increases, just as predicted by the simple model. However, while the predicted curves for the Xe_1 and Xe_2 peaks are nearly the same as for experiment, the experimental slopes for the higher Xe_n change much more drastically with increasing n than those in the hypergeometric ideal mixture. The latter remain fairly steep through $n=7$, unlike the experiment. These detailed differences between the simple model and the experiment are due to those aspects of the distribution of unlike particles into the alpha cages that can be attributed to the differences between Xe–Xe, Xe–Ar, and Ar–Ar interactions, as well as differences between Xe–cage and Ar–cage interactions.

Deviations from ideal mixture behavior

We have used the strictly statistical model derived from the hypergeometric distribution as the limiting case of an ideal mixture for the case where there are exactly eight lattice sites for which both components are competing. We have also offered the GCMC simulations as a more realistic description of the actual system which compares favorably with experiment. Let us now consider specifically the deviations from the ideal mixture behavior.

First let us consider the distribution of Xe and Ar atoms among the cages. There are some interesting comparisons in Table I and Fig. 2:

(a) In the hypergeometric model, for a given $\langle n\rangle_{blue}$, varying $\langle m\rangle_{red}$ has *absolutely no effect* on P_n even though values of $f(n,m)$ changed with the changing $\langle m\rangle_{red}$ since $H_{(n+m)}$ is independent of $\langle n\rangle$ and $\langle m\rangle$. That is, treating Ar as competing equally with Xe for the same eight sites leads to relative spectral intensities that are dependent only on $\langle n\rangle_{Xe}$, not at all on $\langle m\rangle_{Ar}$.

(b) The trends in $[P_n]_{hyp}$ track reasonably well the experimental trends (that is, the envelope of the peaks for Xe_1, Xe_2, Xe_3, Xe_4, Xe_5,...) for the samples with low $\langle n\rangle_{Xe}$, but deviate drastically from experiment at higher Xe loading (5.65 and 6.40).

(c) On close inspection, at low $\langle n\rangle$, the experimental data have a relatively larger fraction of clusters containing 3, 4, and 5 Xe atoms in the coadsorbed real system, than is predicted by the hypergeometric distribution. At high $\langle n\rangle$,

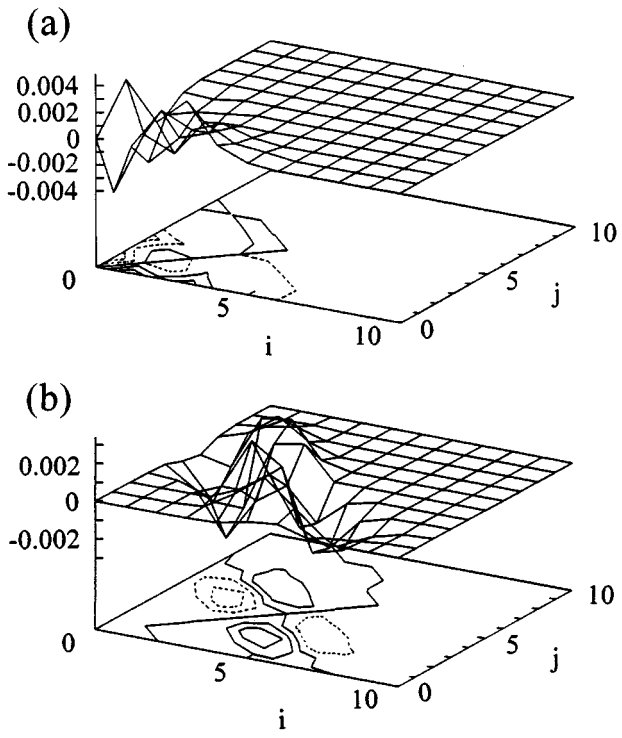

FIG. 11. The difference surface, $[f(\mathrm{Xe}_i\mathrm{Ar}_j)-f(\mathrm{Xe}_j\mathrm{Ar}_i)]$, from GCMC simulations: (a) for low $\langle n\rangle_{\mathrm{Xe}}\cong\langle m\rangle_{\mathrm{Ar}}=0.86$, 0.82 (b) for medium $\langle n\rangle_{\mathrm{Xe}}\cong\langle m\rangle_{\mathrm{Ar}}=3.65$, 3.64. Positive contours are shown as solid curves and negative contours as dashed curves.

the experimental data have a relatively smaller fraction of the smaller clusters and a larger fraction of the larger clusters up to Xe_7. Experimental fractions of Xe_8 are always much smaller than predicted by the hypergeometric distribution.

(d) The $f(n,m)$ predicted by the hypergeometric distribution can be compared with the GCMC results in Fig. 8. Although the general shape of the surface is qualitatively similar, especially for small n and m, the differences between the more realistic GCMC distributions and the ideal mixture distributions become more pronounced at large n.

(e) For the case where $\langle n\rangle=\langle m\rangle$ exactly, the fractions $f(i,j)$ and $f(j,i)$ are exactly equal for all $i\neq j$ pairs in the hypergeometric distribution of blue and red xenon atoms. That is, if the $f(i,j)$ surface is plotted for a given $\langle n\rangle=\langle m\rangle$, the contours would be symmetrical about the 45 deg line. For $\langle n\rangle_{\mathrm{Xe}}=\langle m\rangle_{\mathrm{Ar}}$, we would like to compare GCMC values of $f(\mathrm{Xe}_i\mathrm{Ar}_j)$ with $f(\mathrm{Xe}_j\mathrm{Ar}_i)$ for all $i\neq j$ and see how it is different from the hypergeometric case. In Fig. 11(a) at low loading $\langle n\rangle=\langle m\rangle\sim0.8$, and Fig. 11(b) at higher loading, $\langle n\rangle=\langle m\rangle\sim3.65$ are shown the difference plots $[f(\mathrm{Xe}_i\mathrm{Ar}_j)-f(\mathrm{Xe}_j\mathrm{Ar}_i)]$. In the hypergeometric case the difference plot of $[f(\mathrm{Xe}_i\mathrm{Ar}_j)-f(\mathrm{Xe}_j\mathrm{Ar}_i)]$ should be exactly zero everywhere. The GCMC results, which should be more realistic, show which side of the diagonal has positive contours, that is, those mixed clusters which are favored have slightly larger fractional occurrence than their counterpart. The comparison is made clearer in Table VI where the (i,j) values are listed for those sets in which $[f(\mathrm{Xe}_i\mathrm{Ar}_j)-f(\mathrm{Xe}_j\mathrm{Ar}_i)]>0$. The break-even point seems to be when the total number of particles equals 7. For $(i+j)\leqslant7$, the mixed clusters with the larger number of Xe are preferred, for example, $f(\mathrm{Xe}_4\mathrm{Ar}_2)$ is larger than $f(\mathrm{Xe}_2\mathrm{Ar}_4)$. The deeper Xe–Xe potential well leads to the expected preference for Xe–Xe interactions over Ar–Ar interactions, which make the $\mathrm{Xe}_4\mathrm{Ar}_2$ energetically more favored than its complement $\mathrm{Xe}_2\mathrm{Ar}_4$ when the loadings are the same for Xe and Ar. In contrast, red and blue xenon

TABLE VI. Positive values of $100\times[f(\mathrm{Xe}_i\mathrm{Ar}_j)-f(\mathrm{Xe}_j\mathrm{Ar}_i)]$ for a Xe–Ar mixture in zeolite Na *A* $\langle n\rangle_{\mathrm{Xe}}=\langle m\rangle_{\mathrm{Ar}}=3.65$, obtained from GCMC simulations. Shown are the number of Xe and Ar atoms in the cluster and the values of $[f(\mathrm{Xe}_i\mathrm{Ar}_j)-f(\mathrm{Xe}_j\mathrm{Ar}_i)]>0$.

$i+j$											
1	1,0	0,1									
	none[a]	none									
2	2,0		0,2								
	none		none								
3	3,0	2,1	1,2	0,3							
	0.008	0.005									
4	4,0	3,1		1,3	0,4						
	0.06	0.114									
5	5,0	4,1	3,2	2,3	1,4	0,5					
	0.40	1.07	0.67								
6	6,0	5,1	4,2		2,4	1,5	0.6				
	0.567	2.25	3.38								
7	7,0	6,1	5,2	4,3	3,4	2,5	1,6	0,7			
	0.117	0.923	2.30	1.10							
8	8,0	7,1	6,2	5,3		3,5	2,6	1,7	0,8		
						1.42	1.94	0.38	0.01		
9	9,0	8,1	7,2	6,3	5,4	4,5	3,6	2,7	1,8	0,9	
						1.70	2.20	1.53	0.22	0.02	
10	10,0	9,1	8,2	7,3	6,4		4,6	3,7	2,8	1,9	0,10
	none						0.35	0.50	0.50	0.05	none
11		10,1	9,2	8,3	7,4	6,5	5,6	4,7	3,8	2,9	1,10
							0.003	0.007	0.05	0.085	0.000 09

[a]These clusters were not observed in this GCMC simulation.

atoms are completely equivalent in the ideal mixture hypergeometric model. GCMC simulations show that cages with 5 to 9 argon atoms favor the clusters with the larger number of argon atoms compared to its complement since the Ar atoms are smaller. For example, Xe_2Ar_7 is favored over Xe_7Ar_2. Thus the realistic distributions of the mixed clusters deviate from the strictly statistical distribution in ways that are easy to understand.

Does the presence of Ar affect the distribution of Xe atoms among those cages containing Xe?

As mentioned earlier, the distribution is described by specifying the fraction of all alpha cages containing n Xe atoms (irrespective of the number of Ar atoms), P_n, which can be obtained when $\langle n\rangle_{\mathrm{Xe}}$ is known from mass balance. At loadings $\langle n\rangle_{\mathrm{Xe}}>4.0$, P_0 is essentially zero and P_n is the same as $g(n)$, the fraction of those cages occupied by at least one Xe atom. At lower xenon loadings, the experimental fractions $g(n)$, being directly obtained from the peak areas, have less error than the quantities P_n derived from them. Therefore we will use $g(n)$ rather than P_n in the following discussion. We compare in Fig. 12 the experimental values of $g(n)$ for samples of pure Xe in zeolite Na*A* and for samples of mixtures of Xe and Ar in Na*A*. For reference, we also include the fractions $g(n)$ from the hypergeometric distribution. The hypergeometric distribution gives a reasonably good representation of the distribution at low $\langle n\rangle_{\mathrm{Xe}}$ but not at higher values of $\langle n\rangle_{\mathrm{Xe}}$. As was suggested by Ref. 4, the hypergeometric distribution is a very reasonable model for arriving at the fraction P_0 of empty cages in the pure Xe in Na*A* system. It can be observed in Fig. 12 that the distributions among the filled cages are also reasonably represented by the hypergeometric distribution for $\langle n\rangle_{\mathrm{Xe,\ spectrosc}}<3$, although the systematic deviations are quite clear: the experimental distributions of $g(n)$ vs $\langle n\rangle_{\mathrm{Xe,\ spectrosc}}$ are narrower and more peaked. The results of the GCMC simulations for Xe–Ar mixtures (not shown) agree very well with the experimental data for the Xe–Ar system in the shapes of the $g(n)$ curves and their maxima.

The most striking observation from these experimental data is that the distribution of the Xe atoms *among those cages occupied by Xe atoms* is hardly affected by whether there are also Ar atoms in the cages or not. We see that, within experimental error, the points corresponding to $g(n)$ for Xe in cages of zeolite Na*A* that are also occupied by Ar atoms (●) fall among the points corresponding to $g(n)$ for Xe in the pure Xe in zeolite Na*A* system (□). The differences between these two types of points do not show a systematic trend, and indeed, within the scatter of the experimental data, both sets of points could be fitted to curves resembling the solid curves for the hypergeometric distribution in shape but having the narrower widths and shifted maxima that are found in the GCMC results. For the limiting case of the ideal mixture following the hypergeometric distribution: $\langle n\rangle_{\mathrm{blue,\ spectrosc}}$ is completely independent of the value of $\langle m\rangle_{\mathrm{red}}$. Also, the individual fractions $g(n)$ of those cages occupied by one or more blue particles are exactly the same for samples with the mixed occupancy $\langle n\rangle_{\mathrm{blue}}$ and $\langle m\rangle_{\mathrm{red}}$, for any arbitrary $\langle m\rangle_{\mathrm{red}}$, including $\langle m\rangle_{\mathrm{red}}=0$. Once again, we find that it is convenient to have a model for the limiting case. The actual $g(n)$ values for Xe in mixtures of Xe and Ar in zeolite Na*A* deviate measurably from the values obtained by the hypergeometric distribution, but the invariance of these $g(n)$ with respect to the overall $\langle m\rangle_{\mathrm{Ar}}$ appears to be in agreement with experiment. Other coadsorbates than Ar could lead to a systematic variation of $g(n)$ with respect to the overall $\langle m\rangle$ that may be large

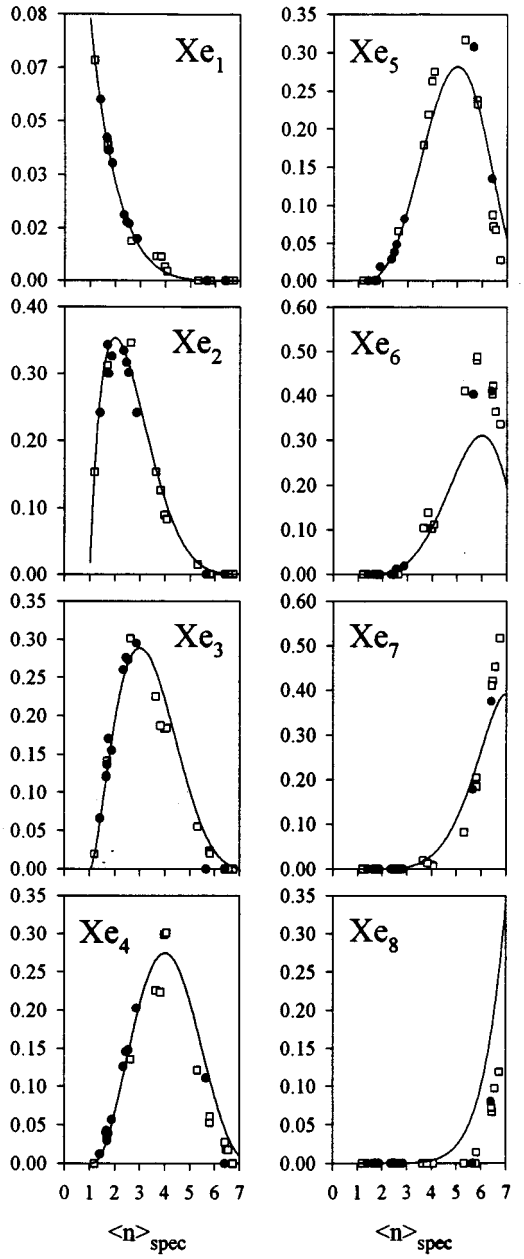

FIG. 12. Experimental equilibrium distribution of Xe atoms at 300 K *among those cages occupied by Xe atoms*. Shown are the fraction $g(n)$ of cages containing Xe_n in samples of zeolite Na*A* containing: (□) pure Xe and (●) a mixture of Xe and Ar. The fractions predicted by the hypergeometric distribution for eight equivalent lattice sites is shown as the solid curve in each case.

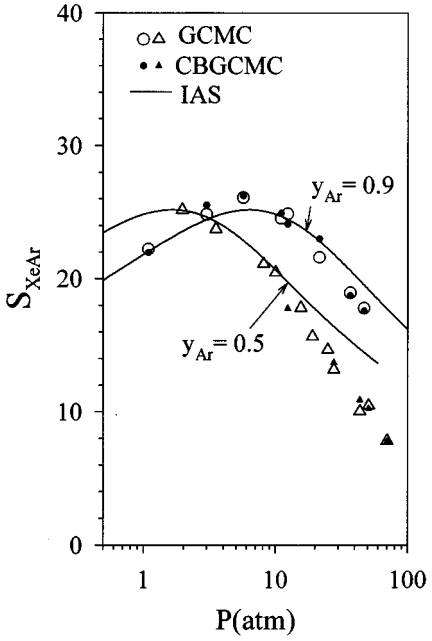

FIG. 13. The selectivity coefficients S_{XeAr} obtained from GCMC simulations by the Norman–Filinov method described in the text and by a cavity-biased sampling method due to Mezei (Ref. 48) (CBGCMC) are compared with the predictions of IAS theory from the adsorption isotherms of pure Xe and Ar. The mole fraction of Ar in the gas phase is y_{Ar}=0.9 (△, ▲) and y_{Ar}=0.5 (○, ●) and all simulations are at 300 K.

enough to observe experimentally. We are currently investigating such examples as CO_2 molecules and other coadsorbates with Xe in Na*A*.

The selectivity coefficient and ideal adsorbed solution theory

The separation factors obtained from GCMC simulations in the binary mixture can be compared with the theoretical separation factors that may be obtained from the individual single-component adsorption isotherms if each component adsorbed independently of the other. In Fig. 13 we show the separation factors or selectivity coefficients from GCMC simulations compared with those calculated from the pure isotherms using ideal adsorbed solution (IAS) theory. We use the conventional definition of selectivity as the ratio of the mole fractions in the zeolite to the ratio of the mole fractions in the bulk.[19,46]

$$S_{\mathrm{Xe,Ar}}=\frac{x_{\mathrm{Xe}}/x_{\mathrm{Ar}}}{y_{\mathrm{Xe}}/y_{\mathrm{Ar}}} \quad \text{or} \quad \frac{\{\langle n\rangle_{\mathrm{Xe}}/\langle m\rangle_{\mathrm{Ar}}\}}{\{\rho_{\mathrm{Xe}}/\rho_{\mathrm{Ar}}\}}.$$

We calculated the spreading pressure π, or rather $(\pi A/RT)$, by integration,

$$(\pi A/RT)=\int_0^p \langle n\rangle_{\mathrm{Xe}}(p)\,\frac{dp}{p}$$

for the pure components using the adsorption isotherms from the GCMC simulations of the pure Xe and pure Ar in zeolite Na*A*. Then from the plots of $(\pi A/RT)$ vs p we obtain at a given total pressure the mole fractions x_{Xe} and y_{Xe}.[19] The agreement of the IAS curves with the actual GCMC results (shown in Fig. 13) for mixtures of Xe and Ar in Na*A* is reasonably good. In previous applications, IAS theory had been successful when the molecular volumes of the two components are nearly the same and/or at low loading.[9,12,18,47] Neither of these conditions hold for our Xe–Ar mixtures in Na*A*. Xe and Ar have very different molecular volumes in our samples ranging from 2.0 to 6.4 atoms per cage. Nevertheless the GCMC results and the predictions of IAS theory in this case are in reasonably good agreement. The same deviations of the GCMC results from IAS theory at high loading are obtained using a particle insertion scheme (suggested by Mezei[48]) that is more efficient for high densities than the standard Norman–Filinov scheme. The results of this cavity-biased sampling method are also shown in Fig. 13.

CONCLUSIONS

We have investigated the Xe–Ar mixture in zeolite Na*A* as a model system for competitive adsorption in microporous solids. For the first time it has been possible to determine experimentally the average number of molecules of the second sorbate occupying the same cage as n atoms of the first sorbate. The Xe_n clusters are trapped in the alpha cages of this zeolite for times sufficiently long that it is possible to observe individual peaks in the NMR spectrum for each cluster while the Ar atoms are in fast exchange between the cages and also with the gas outside. The ^{129}Xe nuclear magnetic resonance spectra of 12 samples of varying Xe and Ar loadings provide detailed information in the form of ^{129}Xe chemical shifts and the intensities of the peaks which are dependent on the average argon and xenon occupancies. Although the detailed distributions, $[f(\mathrm{Xe}_n\mathrm{Ar}_m)$, the fractions of cages containing n Xe atoms and m Ar atoms] have not been observed directly in this system, this information is convoluted into both the observed ^{129}Xe chemical shifts for the Xe_n peaks and the observed distributions P_n, the fraction of cages containing n Xe atoms regardless of the number of Ar atoms. Therefore, these two types of observables provide critical tests for computer simulations of $f(\mathrm{Xe}_n\mathrm{Ar}_m)$. Grand canonical Monte Carlo simulations of mixtures of Xe and Ar in a rigid zeolite Na*A* lattice provide the detailed distributions and the average cluster shifts, as well as the distributions P_n. The agreement with experiment is reasonably good for all 12 samples. The absolute chemical shifts for all the Xe_n peaks observed at 300 K in the 12 samples, spanning a 200 ppm range, are well reproduced by the GCMC simulations.

We have also derived a strictly statistical model of a binary mixture from the hypergeometric distribution, in which the component atoms are distinguishable but equivalent in competition for eight lattice sites per cage under mutual exclusion. This simple model provides a limiting case with which both the GCMC simulations and the actual Xe–Ar system may be compared. This model is found to be very helpful in understanding the experimental observations, for the strictly statistical components of the observed trends

in both the distributions and the ^{129}Xe chemical shifts of the Xe_n peaks can be determined separately and treated in the limiting case of an ideal mixture. Deviations from the ideal mixture behavior are then separately examined, providing additional insight.

This study provides a paradigm for coadsorption in zeolites over a wide range of loadings for adsorbates that have different molecular volumes, providing insight into the distributions of the two types of sorbates *among the cages* as well as their distributions *within a cage*. In this particular system, and indeed in any other system in which the Xe has long residence times while the coadsorbate is fast exchanging between cages, the ^{129}Xe chemical shift and the intensity of each Xe_n peak are quantitative measures of both types of distributions.

ACKNOWLEDGMENTS

This research has been supported by the National Science Foundation (Grant No. CHE92-10790). We are grateful to Professor Rowlinson and M. Maddox, Oxford University, for the core GCMC programs on N_2–CH_4 equimolar binary mixtures which we modified to include binary mixtures of arbitrary composition and calculations of average ^{129}Xe chemical shifts.

[1] *Shape Selective Catalysis in Industrial Applications*, edited by N. Y. Chen, W. E. Garwood, and F. G. Dwyer (Marcel Dekker, New York, 1989) Proceedings of ZEOCAT90, Leipzig, August 1990, Catalysis and Adsorption by Zeolites (Elsevier, Amsterdam, 1990).
[2] *Guidelines for Mastering the Properties of Molecular Sieves: Relationship between the Physicochemical Properties of Zeolitic Systems and their Low Dimensionality*, edited by D. Barthomeuf, E. G. Derouane, and W. Holderich, NATO ASI Ser. 221 (Plenum, New York, 1989).
[3] *Studies in Surface Science and Catalysis, Zeolites and Related Microporous Materials: State of the Art 1994*, edited by J. Weitkamp, H. G. Karge, H. Pfeifer, and W. Holderich (Elsevier, Amsterdam, 1994).
[4] B. F. Chmelka, D. Raftery, A. V. McCormick, L. C. Menorval, R. D. Levine, and A. Pines, Phys. Rev. Lett. **66**, 580 (1991); **67**, 931 (1991).
[5] C. J. Jameson, A. K. Jameson, R. E. Gerald II, and A. C. de Dios, J. Chem. Phys. **96**, 1676 (1992).
[6] C. J. Jameson, A. K. Jameson, B. I. Baello, and H. M. Lim, J. Chem. Phys. **100**, 5965 (1994).
[7] A. K. Jameson, C. J. Jameson, and R. E. Gerald II, J. Chem. Phys. **101**, 1775 (1994).
[8] R. G. Larsen, J. Shore, K. Schmidt-Rohr, L. Emsley, H. Long, A. Pines, M. Janicke, and B. F. Chmelka, Chem. Phys. Lett. **214**, 220 (1993).
[9] R. P. Danner and L. A. Wenzel, A. I. Ch. E. J. **15**, 515 (1969).
[10] D. M. Ruthven, A. I. Ch. E. J. **22**, 753 (1976).
[11] P. Graham, A. D. Hughes, and L. C. V. Rees, Gas Separation and Purification **3**, 56 (1989).
[12] G. W. Miller, K. S. Knaebel, and K. G. Ikels, A. I. Ch. E. J. **33**, 194 (1987).
[13] L. V. C. Rees, J. Hampson, and P. Brueckner, in *Zeolite Microporous Solids: Synthesis, Structure, and Reactivity*, edited by E. G. Derouane *et al.* (Kluwer, Dordrecht, 1992) p. 133.
[14] N. V. Choudary, R. V. Jasra, and S. G. T. Bhat, in *Zeolites and Related Microporous Materials: State of the Art 1994*, Studies in Surface Science and Catalysis, Vol. 84, edited by J. Weitkamp, H. G. Karge, H. Pfeifer, and W. Holderich (Elsevier, Amsterdam, 1994), p. 1247.
[15] C. L. Cavalcante, Jr. and D. M. Ruthven, in *Zeolites and Related Microporous Materials: State of the Art 1994*, Studies in Surface Science and Catalysis, Vol. 84, edited by J. Weitkamp, H. G. Karge, H. Pfeifer, and W. Holderich (Elsevier, Amsterdam, 1994), p. 1209.
[16] E. Rombi, R. Monaci, I. Ferino, V. Solinas, R. Rota, and M. Morbidelli, in *Zeolites and Related Microporous Materials: State of the Art 1994*, Studies in Surface Science and Catalysis, Vol. 84, edited by J. Weitkamp, H. G. Karge, H. Pfeifer, and W. Holderich (Elsevier, Amsterdam, 1994), p. 1355.
[17] R. Hulme, R. E. Rosensweig, and D. M. Ruthven, Ind. Eng. Chem. Res. **30**, 752 (1991).
[18] M. W. Maddox and J. S. Rowlinson, J. Chem. Soc., Faraday Trans. **9**, 3619 (1993).
[19] A. L. Myers and J. M. Prausnitz, A. I. Ch. E. J. **11**, 121 (1965).
[20] F. Karavias and A. L. Myers, Mol. Simul. **8**, 51 (1991).
[21] D. M. Razmus and C. K. Hall, A. I. Ch. E. J. **37**, 769 (1991).
[22] M. W. Maddox, Ph.D. thesis, Oxford University, 1993.
[23] P. R. Van Tassel, H. T. Davis, and A. V. McCormick, Langmuir **10**, 1257 (1994).
[24] B. F. Chmelka, J. G. Pearson, S. B. Liu, L. C. de Menorval, and A. Pines, J. Phys. Chem. **95**, 303 (1991).
[25] J. F. Wu, T. L. Chen, L. J. Ma, M. W. Lin, and S. B. Liu, Zeolites **12**, 86 (1992).
[26] A. Gedeon, T. Ito, and J. Fraissard, Zeolites, **8**, 376 (1988).
[27] A. K. Jameson, C. J. Jameson, A. C. de Dios, E. Oldfield, R. E. Gerald II, and G. L. Turner, Solid State Nucl. Magn. Reson. **4**, 1 (1995).
[28] C. J. Jameson, A. K. Jameson, and S. M. Cohen, J. Chem. Phys. **62**, 4224 (1975).
[29] C. J. Jameson and A. C. de Dios, J. Chem. Phys. **98**, 2208 (1993).
[30] D. W. Breck, W. G. Eversole, R. M. Milton, T. B. Reed, and T. L. Thomas, J. Am. Chem. Soc. **78**, 5963 (1956).
[31] R. J. Harper, G. R. Stifel, and R. B. Anderson, Can. J. Chem. **47**, 4661 (1969).
[32] A. V. Kiselev and P. Q. Du, J. Chem. Soc., Faraday Trans. 2 **77**, 1 (1981).
[33] R. A. Aziz and M. J. Slaman, Mol. Phys. **57**, 825 (1986).
[34] R. A. Aziz and A. van Dalen, J. Chem. Phys. **78**, 2402 (1983).
[35] R. A. Aziz and M. J. Slaman, J. Chem. Phys. **92**, 1030 (1990).
[36] G. C. Maitland, M. Rigby, E. B. Smith, and W. A. Wakeham, *Intermolecular Forces, their Origin and Determination* (Clarendon, Oxford, 1981).
[37] J. J. Pluth and J. V. Smith, J. Am. Chem. Soc. **102**, 4704 (1980).
[38] M. P. Allen and D. J. Tildesley, *Computer Simulation of Liquids* (Clarendon, Oxford, 1987).
[39] G. E. Norman and V. S. Filinov, High Temp. USSR **7**, 216 (1969).
[40] G. B. Woods and J. S. Rowlinson, J. Chem. Soc., Faraday Trans. 2 **85**, 765 (1989).
[41] J. H. Dymond and E. B. Smith, *The Virial Coefficients of Pure Gases and Mixtures* (Clarendon, Oxford, 1980).
[42] J. Brewer, Technical Report. AADD 663448, AFOSR No. 67-2795, Air Force Office of Scientific Research, Arlington, Virginia, 1967.
[43] C. J. Jameson, A. K. Jameson, H. M. Lim, and B. I. Baello, J. Chem. Phys. **100**, 5977 (1994).
[44] G. B. Woods and J. S. Rowlinson, Physica A **164**, 765 (1990).
[45] J. Guemez and S. Velasco, Am. J. Phys. **55**, 154 (1987).
[46] D. M. Ruthven, *Principles of Adsorption and Adsorption Processes* (Wiley, New York, 1984).
[47] G. A. Sorial, W. H. Granville, and W. O. Daly, Chem. Eng. Sci. **38**, 1517 (1983).
[48] M. Mezei, Mol. Phys. **40**, 901 (1980).